first protein that specifically binds to the ion channel modulator.

Xuan et al. have suggested that the majority of human serum PSP94 has a high molecular mass of more than 60 kDa [10]. Later, it was reported that PSP94 binds to a protein in human blood (PSP94-binding protein) [11]. Human PSP94 also exists in a complex with CRISP-3 in seminal fluid [12]. CRISP family proteins are widely distributed in mammals, reptiles [13], and amphibians and are involved in a variety of biological reactions. The N-terminal region of the PSP94-binding protein is homologous to the N-terminal domain of CRISPs.

In order to address the biochemical and physiological functions of the 3 SSPs more thoroughly, the molecular nature of SSPs in Habu serum was examined. Analysis by gel filtration and reverse-phase HPLC revealed that all the SSPs in the serum had high molecular masses of approximately 60 kDa, suggesting the presence of an SSP-binding protein. Identification of the binding molecules will help in the understanding of SSP action. After the purification of the SSP-binding protein from Habu serum, a novel CRISP family protein with sequence homology to triflin was identified. We have examined the structure and property of this protein, which is termed serotriflin. Among the 3 SSPs tested, only SSP-2 formed a stable, noncovalent complex with serotriflin. We will also discuss the role of SSP-2 and serotriflin in Habu blood.

2. Materials and methods

2.1. Materials

We collected blood from *T. flavoviridis* individuals from the Tokunoshima Island by decapitation. The serum was separated by centrifugation and stored at −20 °C. The venom of *T. flavoviridis* was also collected, lyophilized, and stored at −20 °C. Triflin was purified from the venom as described in a previous report [9]. Serum was fractionated with ammonium sulfate into P_{30}–P_{60} as described previously [14]. All the other chemicals were purchased from Wako Pure Chemical Industries Ltd. (Osaka). All experiments with animals were performed in accordance with the ethical standards provided by the International Society in Toxinology [15] and approved by the Institutional Animal Care and Use Committee of Fukuoka University.

2.2. Column chromatography

Analytical gel filtration was carried out using a TSKgel G3000SW column (0.75×30 cm, Tosoh) equilibrated with 0.2 M NaCl–50 mM phosphate buffer (pH 7.0) at a flow rate of 1.0 ml/min. Elution was monitored at 280 nm using an 807-IT integrator. An analytical reverse-phase HPLC was performed on a SepaxBio-C8 column (0.46×25 cm, Sepax Technologies Inc.) with a linear gradient of acetonitrile in 0.1% trifluoroacetic acid at a flow rate of 1.0 ml/min, and elution was monitored at 220 nm.

2.3. Ultrafiltration

Serum fraction P_{60} (1 mg) was dissolved in 150 μl of various buffers: 50 mM NaCl–50 mM citrate buffer (pH 3–6) and 50 mM NaCl–50 mM phosphate buffer (pH 7). After centrifugation at 7000 rpm for 20 min, the residue was removed and the supernatants were transferred to ultrafiltration tubes with a molecular weight cut-off of 30,000 (Ultracel YM-30, Millipore). The tubes were centrifuged at 4000 ×*g* for 30 min, and the retained solution and the ultrafiltrate were separated.

2.4. Sodium dodecyl sulfate-polyacrylamide gel electrophoresis

Sodium dodecyl sulfate-polyacrylamide gel electrophoresis (SDS-PAGE) was carried out on 16.5% polyacrylamide gels under reducing conditions [16]. Ovalbumin (46,000), carbonic anhydrase (30,000), soybean trypsin inhibitor (20,500), lysozyme (14,300), and aprotinin (6500) were used as molecular weight markers. After running the gels under a constant current, they were stained with 0.1% Coomassie brilliant blue R-250 and destained with 10% acetic acid.

2.5. Quantification of proteins

The concentration of pure samples was determined using a spectrophotometer, and the molar extinction coefficients were calculated at 280 nm for SSP-2 (10,595 M^{-1} cm^{-1}), triflin (52,340 M^{-1} cm^{-1}), and serotriflin (46,380 M^{-1} cm^{-1}) [17].

2.6. Purification of SSP-binding protein

Fraction P_{60} (150 mg) was dissolved in a small amount of 0.2 M NaCl–50 mM Tris–HCl (pH 8.0) and loaded on a Sephacryl S-200HR column (2.6×94 cm). Elution was carried out at 4 °C with the same buffer, and 5-ml fractions were collected. Proteins in the second peak were desalted by dialysis and subjected to ion-exchange chromatography using a Q-Sepharose column (1.6×15 cm) equilibrated with 50 mM Tris–HCl (pH 8.0). Elution was performed at 4 °C with a linear gradient of NaCl from 0 to 0.4 M in the same buffer, and 2-ml fractions were collected. Proteins in the second peak were collected, desalted by dialysis, and subjected to reverse-phase HPLC. An analytical run was carried out using a column of Cosmosil-5C_8-AR-300 (0.46×15 cm, Nacalai tesque). Elution was carried out with an appropriate gradient of acetonitrile in 0.1% trifluoroacetic acid at a flow rate of 1.0 ml/min and was monitored at 230 nm. For the preparation of SSP-binding protein, a YMC-Pack C8 column (1.0×25 cm, YMC) was used at a flow rate of 3.0 ml/min. The effluent containing the SSP-binding protein was collected, and the pH was immediately adjusted to 8.5 by the addition of 0.5 M Tris–HCl (pH 8.5).

2.7. Mass spectrometric analysis

Mass spectrum was measured on a Voyager DE-STR MALDI-TOF-mass spectrometer (PerSeptive Biosystems). The sample was dissolved in 0.1% trifluoroacetic acid–50% acetonitrile containing α-cyano-4-hydroxycinnamic acid (10 mg/ml) as the matrix, and 2-μl aliquots were analyzed. The spectrum was calibrated with the molecular mass of apomyoglobin.

2.8. Protein sequence analysis

Serotriflin was reduced and *S*-pyridylethylated according to Friedman et al. [18]. The *S*-pyridylethylated protein (400 μg each) was digested at 37 °C with Lys-C (E/S=1:90) for 6 h in 2 M urea–50 mM Tris–HCl (pH 9.0), α-chymotrypsin (E/S=1:100) for 4 h in 1 M urea–50 mM NH_4HCO_3, or Asp-N (E/S=1:100) for 16 h in 1.6 M urea–20 mM phosphate buffer (pH 8.0). The digests were lyophilized and fractionated by reverse-phase HPLC on a YMC-Pack ODS column (0.46×25 cm, YMC) in 0.1% trifluoroacetic acid with an appropriate gradient of acetonitrile. The amino acid sequences of proteins and peptides were determined by the automatic protein sequencing system PPSQ 21.

2.9. Cloning of cDNA fragment encoding the serotriflin precursor

Total RNA was extracted from the liver of *T. flavoviridis* by the acid guanidinium-phenol-chloroform method and reverse-transcribed to synthesize cDNA first strands using an adaptor-linked oligo(dT) primer (5'-GGCCAC-GCGTCGACTAGTAC(dT)$_{17}$-3'). The resultant cDNAs were used as a template for the 3'-rapid amplification of cDNA ends (RACE) reaction. Synthetic oligonucleotides, namely, *Srtf-sig* (5'-GCTGCAGTGCTGCAACAGTCTTCT-GGAAC-3') and *3'-Adp* (5'-GGCCACGCGTCGACTAGTAC-3'), were used for PCR amplification. The *Srtf-sig* primer was designed based on the signal sequence of triflin [9], and *3'-Adp* corresponded to the adaptor sequence within the adaptor-linked oligo(dT) primer. The amplification product was subcloned into the plasmid vector pBluescript II. The nucleotide sequences of cDNA inserts were determined using ABI PRISM 377 DNA Sequencing System (Applied Biosystems).

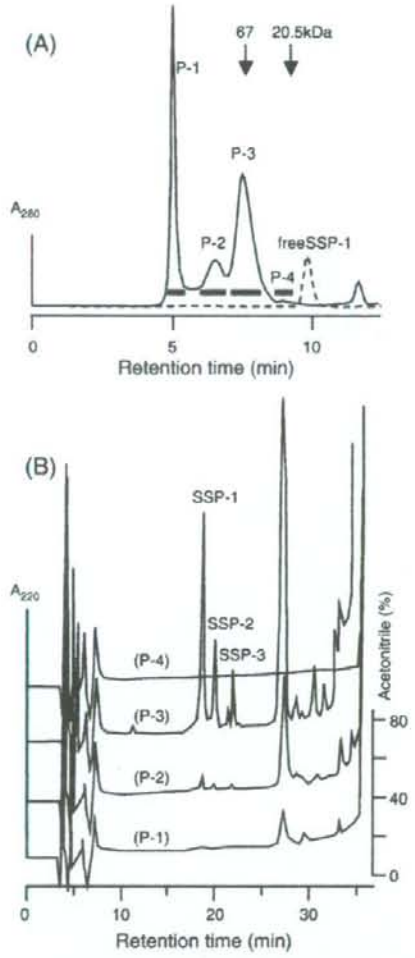

Fig. 1. Analysis of molecular states of SSPs in Habu serum. (A) Analytical gel filtration of *T. flavoviridis* serum (solid line) and SSP-1 (broken line). Either the serum (10 μl) or 500 μM of purified SSP-1 (10 μl) was applied to a column of TSKgel G3000SW (0.75×30 cm) equilibrated with 0.2 M NaCl–50 mM phosphate buffer (pH 7.0). (B) Reverse-phase HPLC on a column of SepaxBio-C8 (0.46×25 cm) of fractions P-1, P-2, P-3, and P-4.

2.10. Binding assay of SSPs and serotriflin

A constant amount of serotriflin was mixed with various amounts of SSP-1, SSP-2, and SSP-3 in 1.0 M NaCl–50 mM phosphate buffer (pH 7.0). After the mixture was left at room temperature for 10 min, the aliquots were subjected to analytical gel filtration as described above except that 1.0 M NaCl–50 mM phosphate buffer (pH 7.0) was used as the eluent. Elution was monitored at 280 nm, and the peak area was determined using an 807-IT integrator (Jasco). Column was calibrated by bovine serum albumin (67,000), ovalbumin (46,000), and soybean trypsin inhibitor (20,500).

2.11. Surface plasmon resonance analysis of binding kinetics

Kinetic measurements of the interaction between SSP and triflin/serotriflin were performed using a Biacore 2000 instrument (Biacore). The flow cells of CM5 sensor chips were activated with 100 μl of 0.2 M 1-ethyl-3-(3-dimethylaminopropyl)carbodiimide and 0.05 M *N*-hydroxysuccinimide at a flow rate of 10 μl/min. SSP-2 at a concentration of 10 μg/ml in 10 mM sodium acetate buffer (pH 4.0) was injected to reach 500 resonance units (RU), and the unreacted groups were blocked with 20 μl of 1 M ethanolamine (pH 8.5). SSP-1 was used as a negative control protein. The analytes, diluted to various concentrations in 10 mM Hepes–0.15 M NaCl–3 mM EDTA–0.005% surfactant P20 (pH 7.4), were injected for 90 s during the association phase at a constant flow rate of 20 μl/min. The dissociation was subsequently followed for 180 s at the same flow rate. The surface of the sensor chip was regenerated using 10 mM Gly–HCl buffer (pH 2.0) after the binding of analyte. The sensograms were corrected by subtraction of the signal from the negative control surface and used to calculate the rate and affinity constants by using BiaEvaluation 4.1 (Biacore AB) and Origin 5.0 (Microcal).

3. Results

3.1. Analysis of molecular states of SSPs in Habu serum

Small proteins in serum, such as SSPs, likely to be easily excreted in the urine if freely present in plasma in its monomeric form. To determine the native molecular status of SSPs, we first attempted to estimate their molecular mass by a gel filtration of native Habu serum proteins. Analytical gel filtration using a TSKgel G3000SW column showed that SSP-1 was eluted at 9.88 min (Fig. 1A). However, when Habu serum was analyzed in the same manner, 4 protein peaks (P-1–P-4) appeared at 5.03, 6.75, 7.85, and 8.86 min, but no peak was observed near 10 min. To examine the presence of SSPs after gel filtration, 4 fractions containing peaks P-1–P-4 were collected and subjected directly to an analytical reverse-phase HPLC. As shown in Fig. 1B, most of the SSPs were detected in fraction P-3. The apparent molecular mass of P-3 was approximately 60 kDa. This result clearly indicates that the SSPs are not in a free state but exist in the high molecular mass form in Habu serum. Since SSPs do not form any oligomer in physiological buffers, the presence of an SSP-binding protein is suggested.

3.2. Property of SSP–protein complex

In order to identify the SSP-binding protein, some properties of the SSP–protein complex were examined. An ammonium sulfate fraction (P_{60}) was dissolved in buffers at pH 3–7 and

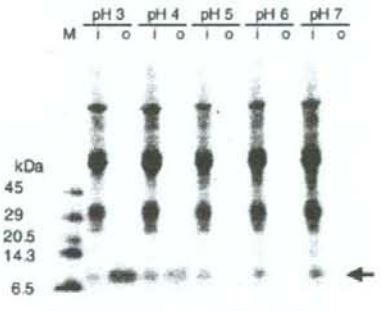

Fig. 2. pH-dependent dissociation of the SSP–protein complex. The pH of *T. flavoviridis* serum was adjusted with the addition of buffers (pH 3–7), and the mixture was filtered through an ultrafiltration membrane of molecular weight cut-off of 30,000. The inner solution (*i*) and the outer ultrafiltrate (*o*) were analyzed by SDS-PAGE. M, marker proteins. An arrow indicates the position of SSPs.

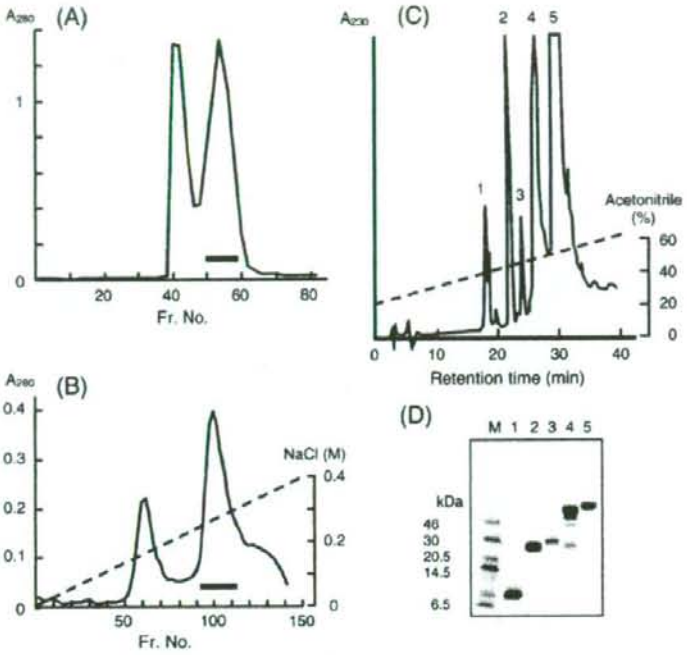

Fig. 3. Purification of the SSP-binding protein. (A) Gel filtration of an ammonium sulfate fraction (P_{60}) from *T. flavoviridis* serum on a Sephacryl S-200HR column. Fractions indicated by a bar were collected. (B) Q-Sepharose chromatography of the sample obtained from gel filtration. Fractions indicated by a bar were collected. (C) Reverse-phase HPLC of the sample obtained from Q-Sepharose chromatography on a Cosmosil-5C_8-AR-300 column. (D) SDS-PAGE of the samples obtained from the peaks 1–5 by reverse-phase HPLC. M, a mixture of marker proteins.

subjected to ultrafiltration with a membrane having a molecular weight cut-off of 30,000. The inner (retained) solutions and the outer ultrafiltrates were then analyzed by SDS-PAGE (Fig. 2). SSPs were retained on the membrane in solutions above pH 5. On the other hand, SSPs were detected in the outer solutions below pH 4, and a small amount of SSPs were present in the ultrafiltrates. No other protein band of above 10 kDa was detected. This indicates that the SSP–protein complex dissociates in acidic solutions, and the SSP-binding protein cannot pass through the membrane.

3.3. Identification of SSP-binding protein

The SSP–protein complex was purified from P_{60} by gel filtration and anion-exchange chromatography. The gel filtration of P_{60} resulted in 2 peaks on a Sephacryl S-200HR column (Fig. 3A). SSPs were detected only in the second peak. This material was further purified by anion-exchange chromatography on a Q-Sepharose column, resulting in 2 major peaks (Fig. 3B). Since the second peak contained the highest amount of SSPs, the components in this peak were examined by reverse-phase HPLC on a C8 column (Fig. 3C). Under the acidic conditions used in this chromatography, SSPs could be liberated from the complex, and 5 major peaks were detected. SDS-PAGE analysis revealed that peaks 1, 2, and 5 corresponded to SSP-1, PLI-I [19], and serum albumin, respectively (Fig. 3D). Peak 4 was formed by a mixture of at least 4 proteins, including PLI-II [19] and HSF [14]. Peak 3 corresponded to a single protein having a molecular mass of approximately 30 kDa. MALDI-TOF-mass spectrometry revealed the exact mass of this protein to be 27,645.7 Da. The protein recovered from peak 3 was directly subjected to N-terminal sequence analysis, yielding the following 39 residues: TVDFASESAN ERETQ-KEILD KHNALRRSVR PTARNMLQM. Since a similarity

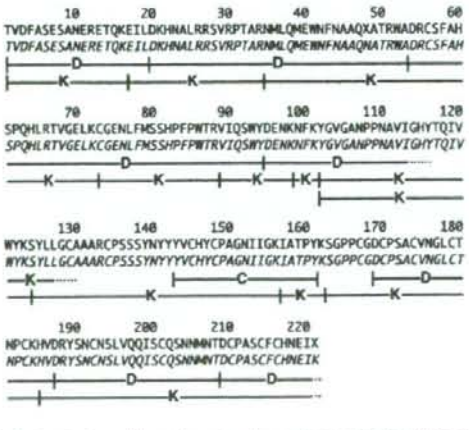

Fig. 4. Determination of the primary structures of serotriflin. D, Asp-N digests; K, Lys-C digests; C, chymotrypsin digests.

was observed between this sequence and that of triflin [9] from *T. flavoviridis* venom, this new protein was termed serotriflin. The primary structure of serotriflin was determined by protein sequencing. *S*-pyridylethylated serotriflin was digested by Asp-N, Lys-C, or chymotrypsin, and the amino acid sequences of fragment peptides were determined (Fig. 4). We could determine the entire sequence except for residues 48 and 221 (the C-terminal residue). To elucidate the amino acid sequence of the serotriflin precursor, we cloned the cDNA-encoding serotriflin precursor from the liver of *T. flavoviridis*. The result is shown in Fig. 4 in italics. The C-terminal amino acid was assigned to be Lys. As was expected, residue 48 was Asn. The sequence Asn^{48}-X-Thr^{50} may suggest that a sugar chain is attached to this residue.

3.4. Binding analysis of serotriflin with SSPs

In a previous paper, we reported that triflin can selectively bind to SSP-2 [7]. High similarity between the sequences of both triflin and serotriflin suggested that serotriflin could also bind to some SSPs. Native serotriflin was purified as described above. At the final step of purification, the pH of the effluent was immediately adjusted to 8.5 by the addition of 0.5 M Tris–HCl (pH 8.5) since prolonged storage in an acidic solution may denature serotriflin. Lyophilization and desalting with dialysis revealed that the native serotriflin and its circular dichroism (CD) spectrum were considerably similar to native triflin and its CD spectrum, respectively (data not shown). In order to examine the possibility of serotriflin being the SSP-binding protein in Habu serum, we first tested the binding of serotriflin to the 3 SSPs by using the same method of native PAGE as that used for the binding analysis of triflin [7]. However, we could not detect any band of serotriflin by this method since serotriflin is a basic protein with a calculated p*I* of 8.8 and does not enter the gel under standard conditions [20]. Therefore, the binding was monitored by analytical gel filtration. Because serotriflin was eluted at an apparent molecular weight of 16,000 in a solvent containing 0.2 M NaCl, elution was performed with a buffer containing 1.0 M NaCl to eliminate the unordinary interaction between the protein and the gel matrix. Various amounts of SSPs were mixed with serotriflin and the mixtures were analyzed by gel filtration: serotriflin, SSP-1, SSP-2, and SSP-3 were eluted at 9.76, 10.73, 10.90, 11.35 min, respectively. When the molar ratio of SSP-2/serotriflin was less than 1, a shoulder was observed at 9.32 min (Fig. 5). When more than 1 equivalent of SSP-2 was mixed with serotriflin, the 9.32-min peak (peak **a** in Fig. 5) was the major one, and a peak appeared at 10.90 min (peak **c**) due to excess SSP-2. Peak **a** was assumed

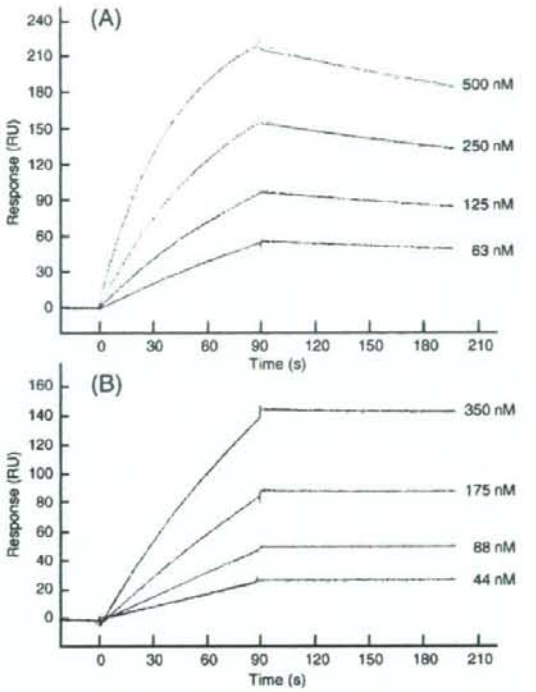

Fig. 6. Surface plasmon resonance analyses of the binding of SSP-2 to CRISP family proteins. Representative data of equilibrium binding of triflin (A) and serotriflin (B) to SSP-2. Serially diluted serotriflin (from 500 to 63 nM for triflin and from 350 to 44 nM for serotriflin) were injected at a flow rate of 20 μl/min through flow cells with the SSP-2 immobilized to the sensor chip surface at 500 RU.

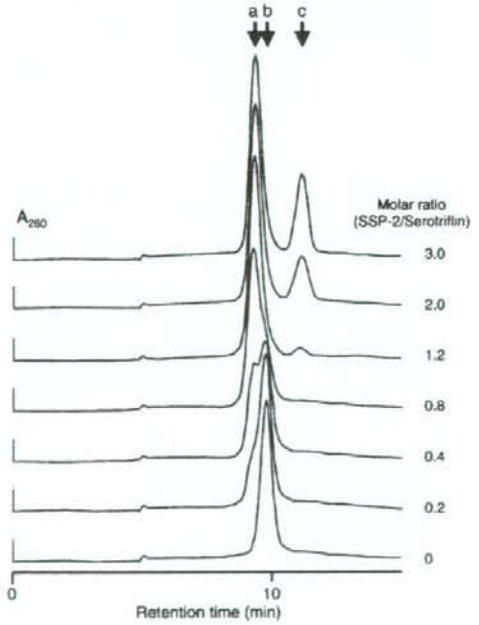

Fig. 5. Binding of SSP-2 to serotriflin. To a constant amount of serotriflin (40 μM) were added varing amounts of SSP-2, and the mixtures were analyzed by gel filtration HPLC on a column of TSKgel G3000SW (0.75 × 30 cm) in 1.0 M NaCl–50 mM phosphate buffer (pH 7.0) with a flow rate of 1.0 ml/min. Arrows indicate the positions of serotriflin–SSP-2 complex (**a**), serotriflin (**b**), and SSP-2 (**c**).

Table 1
Surface plasmon resonance analyses of the binding of serotriflin and triflin to immobilized SSP-2

Ligand	Analyte	k_a (1/Ms)	k_d (1/s)	K_D (M)
SSP-2	Triflin	$5.42\pm0.65\times10^{4}$	$1.26\pm0.04\times10^{-3}$	$2.40\pm1.14\times10^{-8}$ ($1.76–3.25\times10^{-8}$)
SSP-2	Serotriflin	$4.00\pm0.38\times10^{3}$	$8.65\pm0.12\times10^{-5}$	$2.15\pm0.36\times10^{-8}$ ($1.86–2.68\times10^{-8}$)

The kinetics of the interaction between SSP-2 and CRISP family proteins (triflin and serotriflin) was evaluated with a Biacore 2000 instrument. The ligand SSP-2 was immobilized on a surface that was challenged with different concentrations of serotriflin and triflin, and association and dissociation rates (k_a and k_d) were measured. The average values of four independent experiments are cited. The range of equilibrium dissociation constants (K_D) are given in parentheses.

to be formed by a complex between SSP-2 and serotriflin because its molecular weight was estimated to be 37,000 by a calibration curve. On the other hand, SSP-1 and SSP-3 resulted in 2 peaks corresponding to free serotriflin and each of the SSPs, and no peak corresponding to the complex with serotriflin could be detected (data not shown).

3.5. Kinetics of complex formation between SSP-2 and triflin or serotriflin

The SSP-2–triflin complex is stable and does not dissociate during native PAGE analysis [7]. The gel filtration experiments described above also show the stable nature of the SSP-2–serotriflin complex. The affinity between the SSPs and the 2 CRISP proteins was further examined in detail by continuous monitoring of binding and dissociation by surface plasmon resonance technology. Preliminary experiments using the 3 SSPs have indicated that SSP-1 and SSP-3 do not bind to triflin and serotriflin (data not shown). Therefore, SSP-1 was selected as a negative control protein in the surface plasmon resonance experiments. The affinity of SSP-2 was evaluated for triflin (Fig. 6A) and serotriflin (Fig. 6B). The sensograms reveal that both proteins have high affinity with SSP-2, as indicated by the low dissociation rates. Global evaluation using the 1:1 Langmuir binding model yielded kinetic binding parameters of the 2 proteins (Table 1). The association rate (k_a) of SSP-2 for triflin was approximately 10 times higher than that for serotriflin, but the dissociation of the SSP-2–serotriflin complex was considerably slower than the complex with triflin. The low dissociation constants (K_D) also suggest that the interactions between the 2 proteins and SSP-2 are highly specific.

4. Discussion

Even though PSP94 was first isolated as a major protein from human seminal plasma [21], it was later found to be present at the same level in women as that in men [22]. Besides its roles in fertility [23,24], several functions have been postulated to this protein [25,26]. PSP94 family proteins have been isolated from pig [2], monkey [4,6,27], mouse [3], rat [28], and ostrich [5]. They are composed of 91–94 amino acids, have 10 highly conserved cysteine residues, and remain quite stable on heating and at extreme pH values [29]. Recently, it was reported that human PSP94 exists as the complex with PSP94-binding protein (PSPBP) in the blood [11]. PSPBP is a glycosylated protein, and the N-terminal region within the human PSPBP showed sequence similarity (more than 40% identity) with a defined family of proteins having the sperm coating glycoprotein (SCP)-like domain [30]. The CRISP family protein also has the SCP domain. The PSPBP can be considered to be a member of this family. Udby et al. [12] reported that human PSP94 also exists as a complex with CRISP-3 in seminal fluid. Since SSPs are low molecular mass proteins belonging to the PSP94 family, they may also be present in a high molecular mass form. Gel filtration analysis of *Habu* serum clearly indicated that all the SSPs have molecular masses higher than the monomeric protein. The presence of a binding protein with a high molecular mass can be expected in the serum. Serotriflin has been isolated from *Habu* serum as a candidate for an SSP-binding protein. Structural analysis by peptide sequencing as well as cDNA cloning has proved that this new protein is a member of the CRISP family. This family of proteins shows a wide phylogenetic distribution, ranging from plants to mammals, and is characterized by the presence of conserved cysteine residues

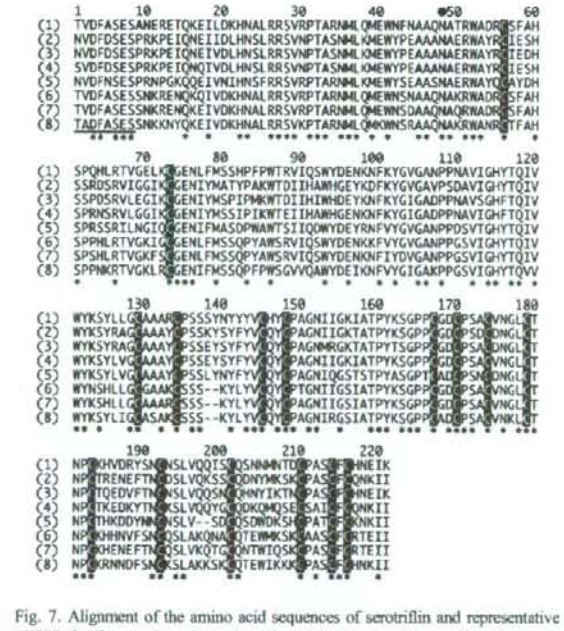

Fig. 7. Alignment of the amino acid sequences of serotriflin and representative CRISP family members from several snake venoms. Conserved residues are indicated by asterisks. Cysteine residues are shown in white-on-black. For each CRISP member sequence, corresponding GenBank accession number and percent identity to serotriflin are as follows: (1) serotriflin; (2) triflin (AAM45665, 68%); (3) ablomin (AAM45664, 69%); (4) piscivorin (AAO62994, 71%); (5) tigrin (AAM19739, 65%); (6) natrin-2 (Q7ZZN8, 79%); (7) latisemin (AAM45666, 81%); (8) pseudochetoxin (Q8AVA4, 73%). Propeptide of pseudochetoxin is underlined.

[13]. Several CRISP proteins have been associated with crucial biological processes such as gamete maturation, fertilization and host defense responses [31]. However, the functions of most CRISPs remain unknown. Serotriflin has 16 cysteine residues and is highly homologous to several CRISP proteins from a variety of snake venoms as shown in Fig. 7. When the amino acid sequence of serotriflin was compared with that of trifling — a snake venom CRISP that inhibits smooth muscle contraction by inhibiting the Ca^{2+} channel [9], the sequence identity was 65% in the mature protein region. Both the proteins are composed of 221 residues, whereas the molecular masses of triflin and serotriflin were determined to be 24,803.5 and 27,645.7 Da, respectively, by MALDI-TOF-mass spectrometry. The larger molecular mass of serotriflin is attributable to the presence of a sugar chain at Asn48. In the cloning experiments, we used a primer that was designed based on the signal sequence of triflin for PCR amplification. It is likely that the signal peptide of serotriflin may be quite similar to that of triflin. Although many CRISP family members have been identified as the venomous proteins, serotriflin is the first CRISP family protein found in snake serum.

In spite of the sequence similarity between triflin and serotriflin, the latter must have no toxic activity such as the Ca^{2+} channel-blocking activity. On the basis of the crystallographic study of CRISPs, Morita et al. have shown that triflin is composed of 2 domains and hydrophobic residues (including Phe189, Leu 195, Tyr205, and Phe215), which may obstruct the target ion channel and are exposed to the solvent [32]. They also proposed the significance of 2 residues, namely, Glu186 and Phe189, as the most likely functional residues. In serotriflin, these residues are replaced by Val186 and Tyr189 (Fig. 7). Moreover, no homology between triflin and serotriflin can be observed at residues 184–190, which is thought to be a possible interaction site. This may support the above suggestion of the ion-channel-blocking activity of triflin, and serotriflin appears to have no such activity.

The complexes between SSPs and their binding proteins could dissociate in acidic solutions below pH 4 (Fig. 2). When P_{60} was dissolved in a buffer with pH 7.4 and subjected to ultrafiltration, no SSP was recovered in the ultrafiltrate. In contrast, the ultrafiltrate of P_{60} at pH 3.5 contained 3 SSPs as the main components when analyzed by reverse-phase HPLC (data not shown). SSPs purified by HPLC at pH 2 had complete activity, as judged by either metalloproteinase inhibition [7] or binding affinity to triflin. The SSPs are considerably stable to extreme pH values as well as high temperatures (data not shown). This property may be attributable to the tight conformation of SSPs as estimated from the 3D structure of human and porcine PSP94 [33]. The acid stability of SSPs facilitated the Biacore experiments; repeated washing of the sensor chip conjugating the SSP-2 with a buffer at pH 2 indicated no decrease in the binding potency to triflin or serotriflin. The gel filtration experiment suggested that the stoichiometry of serotriflin and SSP-2 in the complex is 1:1 (Fig. 5). This is in contrast to the 2:1 stoichiometry between human PSP94 and CRISP-3 [12]. Both triflin and serotriflin were bound to SSP-2 with high affinity; the dissociation constants for the SSP-2–triflin and SSP-2–serotriflin complexes were 24.0 and 21.5 nM, respectively. The k_a and k_d of SSP bound to serotriflin were both approximately 10–150 times lower than those of SSP bound to triflin. This indicates that serotriflin is an excellent carrier protein for SSP-2. As described above, SSP-2 may exist as a complex with serotriflin. If SSP-2 can bind to triflin instead of serotriflin in blood serum and suppress the toxic activity of triflin, SSP-2 may play a role in the defense system of venomous snakes in the case of self-envenomation. Unlike SSP-2, other SSPs could not effectively bind to serotriflin or to triflin; however, they also exist in high molecular mass forms (Fig. 1). Since SSP-1 and SSP-3 do not aggregate in aqueous buffers, another binding protein should be present in *Habu* serum. The identification of such a protein is currently underway.

References

[1] J.Y. Dube, G. Frenette, R. Paquin, P. Chapdelaine, J. Tremblay, R.R. Tremblay, C. Lazure, N. Seidah, M. Chretien, Isolation from human seminal plasma of an abundant 16-kDa protein originating from the prostate, its identification with a 94-residue peptide originally described as β-inhibin, J. Androl. 8 (1987) 182–189.

[2] P. Fernlund, L.B. Granberg, P. Roepstor, Amino acid sequence of β-microseminoprotein from porcine seminal plasma, Arch. Biochem. Biophys. 309 (1994) 70–76.

[3] J.W. Xuan, J. Kwong, F.L. Chan, M. Ricci, Y. Imasato, H. Sakai, G.H. Fong, C. Panchal, J.L. Chin, cDNA, genomic cloning, and gene expression analysis of mouse PSP94 (prostate secretory protein of 94 amino acids), DNA Cell Biol. 18 (1999) 26.

[4] M. Makinen, C. Valtonen-Andre, A. Lundwall, New world, but not old world, monkeys carry several genes encoding β-microseminoprotein, Eur. J. Biochem. 264 (1999) 407–414.

[5] C. Lazure, M. Villemure, D. Gauthier, R.J. Naude, M. Mbikay, Characterization of ostrich (*Struthio camelus*) β-microseminoprotein (MSP): identification of homologous sequences in EST databases and analysis of their evolution during speciation, Protein Sci. 10 (2001) 2207–2218.

[6] S. Nolet, D. St-Louis, M. Mbikay, M. Chretien, Rapid evolution of prostatic protein PSP94 suggested by sequence divergence between rhesus monkey and human cDNAs, Genomics 9 (1991) 775–777.

[7] N. Aoki, A. Sakiyama, M. Deshimaru, S. Terada, Identification of novel serum proteins in a Japanese viper: homologs of mammalian PSP94, Biochem. Biophys. Res. Commun. 359 (2007) 330–334.

[8] S. Fujimura, K. Oshikawa, S. Terada, E. Kimoto, Primary structure and autoproteolysis of brevilysin H6 from the venom of *Gloydius halys brevicaudus*, J. Biochem. 128 (2000) 167–173.

[9] Y. Yamazaki, H. Koike, Y. Sugiyama, K. Motoyoshi, T. Wada, S. Hishinuma, M. Mita, T. Morita, Cloning and characterization of novel snake venom proteins that block smooth muscle contraction, Eur. J. Biochem. 269 (2002) 2708–2715.

[10] D. Wu, Y. Guo, A.F. Chambers, J.I. Izawa, J.L. Chin, J.W. Xuan, Serum bound forms of PSP94 (prostate secretory protein of 94 amino acids) in prostate cancer patients, J. Cell. Biochem. 76 (1999) 71–83.

[11] J.R. Reeves, J.W. Xuan, K. Arfanis, C. Morin, S.V. Garde, M.T. Ruiz, J. Wisniewski, C. Panchal, J.E. Tanner, Identification, purification and characterization of a novel human blood protein with binding affinity for prostate secretory protein of 94 amino acids, Biochem. J. 385 (2005) 105–114.

[12] L. Udby, A. Lundwall, A.H. Johnsen, P. Fernlund, C. Valtonen-Andre, A.M. Blom, H. Lilja, N. Borregaard, L. Kjeldsen, A. Bjartell, β-microseminoprotein binds CRISP-3 in human seminal plasma, Biochem. Biophys. Res. Commun. 333 (2005) 555–561.

[13] Y. Yamazaki, T. Morita, Structure and function of snake venom cysteine-rich secretory proteins, Toxicon 44 (2004) 227–231.

[14] M. Deshimaru, C. Tanaka, A. Tokunaga, M. Goto, S. Terada, Efficient method for purification of antihemorrhagic factor (HSF) in the serum of Japanese Habu (*Trimeresurus flavoviridis*), Fukuoka Univ. Sci. Rep. 33 (2003) 45–53.

[15] International Society of Toxinology, Instructions for contributors to Toxicon, Toxicon 31 (1993) 9–11.
[16] H. Schagger, G. von Jagow, Tricine-sodium dodecyl sulfate-polyacrylamide gel electrophoresis for the separation of proteins in the range from 1 to 100 kDa, Anal. Biochem. 166 (1987) 368–379.
[17] S.C. Gill, P.H. von Hippel, Calculation of protein extinction coefficients from amino acid sequence data, Anal. Biochem. 182 (1989) 319–326.
[18] M. Friedman, L.H. Krull, J.F. Cavins, The chromatographic determination of cystine and cysteine residues in proteins as *S*-β-(4-pyridylethyl) cysteine, J. Biol. Chem. 245 (1970) 3868–3871.
[19] I. Nobuhisa, S. Inamasu, M. Nakai, A. Tatsui, T. Mimori, T. Ogawa, Y. Shimohigashi, Y. Fukumaki, S. Hattori, H. Kihara, M. Ohno, Structural elements of *Trimeresurus flavoviridis* serum inhibitors for recognition of its venom phospholipase A_2 isozymes, Eur. J. Biochem. 249 (1997) 838–845.
[20] B.J. Davis, Disc electrophoresis II. Method and application to human serum proteins, Ann. N. Y. Acad. Sci. 121 (1964) 404–427.
[21] H. Lilja, P.A. Abrahamsson, Three predominant proteins secreted by the human prostate gland, Prostate 12 (1988) 29–38.
[22] H. von der Kammer, E. Krauhs, G. Aumuller, K.H. Scheit, Characterization of a monoclonal antibody specific for prostatic secretory protein of 94 amino acids (PSP94) and development of a two-site binding enzyme immunoassay for PSP94, Clin. Chim. Acta 187 (1990) 207–219.
[23] A.R. Sheth, N. Arabatti, M. Carlquist, H. Jornvall, Characterization of a polypeptide from human seminal plasma with inhibin (inhibition of FSH secretion)-like activity, FEBS Lett. 165 (1984) 11–15.
[24] C.F. Chao, S.T. Chiou, H. Jeng, W.C. Chang, The porcine sperm motility inhibitor is identical to β-microseminoprotein and is a competitive inhibitor of Na^+,K^+-ATPase, Biochem. Biophys. Res. Commun. 218 (1996) 623–628.
[25] S.V. Garde, V.S. Basrur, L. Li, M.A. Finkelman, A. Krishan, L. Wellham, E. Ben-Josef, M. Haddad, J.D. Taylor, A.T. Porter, D.G. Tang, Prostate secretory protein (PSP94) suppresses the growth of androgen-independent prostate cell line (PC3) and xenografts by inducing apoptosis, Prostate 38 (1999) 118–125.
[26] N. Shukeir, A. Arakelian, S. Kadhim, S. Garde, S.A. Rabbani, Prostate secretory protein (PSP-94) decreases tumor growth and hypercalcemia of malignancy in a syngenic in vivo model of prostate cancer, Cancer Res. 63 (2003) 2072–2078.
[27] J.W. Xuan, D. Wu, Y. Guo, S. Garde, D.T. Shum, M. Mbikay, R. Zhong, J.L. Chin, Molecular cloning and gene expression analysis of PSP94 (prostate secretory protein of 94 amino acids) in primates, DNA Cell Biol. 16 (1997) 627–638.
[28] P. Fernlund, L.B. Granberg, I. Larsson, Cloning of β-microseminoprotein of the rat: a rapidly evolving mucosal surface protein, Arch. Biochem. Biophys. 334 (1996) 73–82.
[29] I. Wang, T.A. Yu, S.H. Wu, W.C. Chang, C. Chen, Disulfide pairings and secondary structure of porcine β-microseminoprotein, FEBS Lett. 541 (2003) 80–84.
[30] N. Mizuki, M. Kasahara, Mouse submandibular glands express an androgen-regulated transcript encoding an acidic epididymal glycoprotein-like molecule, Mol. Cell. Endocrine. 89 (1992) 25–32.
[31] T. Szyperski, C. Fernandez, C. Mumenthaler, K. Wuthrich, Structure comparison of human glioma pathogenesis-related protein GliPR and the plant pathogenesis-related protein P14a indicates a functional link between the human immune system and a plant defense system, Proc. Nat. Acad. Sci. U. S. A. 95 (1998) 2262–2266.
[32] Y. Shikamoto, K. Suto, Y. Yamazaki, T. Morita, H. Mizuno, Crystal structure of a CRISP family Ca^{2+}-channel blocker derived from snake venom, J. Mol. Biol. 350 (2005) 735–743.
[33] H. Ghasriani, K. Teilum, Y. Johnsson, P. Fernlund, T. Drakenberg, Solution structures of human and porcine β-microseminoprotein, J. Mol. Biol. 362 (2006) 502–515.

ELSEVIER

Experimental Hematology

Experimental Hematology 2008;36:897–906

Growth and maturation of megakaryocytes is regulated by Lnk/Sh2b3 adaptor protein through crosstalk between cytokine- and integrin-mediated signals

Hitoshi Takizawa[a,c,*], Koji Eto[b], Atsuko Yoshikawa[c], Hiromitsu Nakauchi[b], Kiyoshi Takatsu[a,d,e], and Satoshi Takaki[c]

[a]*Division of Immunology, Department of Microbiology and Immunology;* [b]*Laboratory of Stem Cell Therapy, Center for Experimental Medicine, The Institute of Medical Science, The University of Tokyo, Tokyo, Japan;* [c]*Research Institute, International Medical Center of Japan, Tokyo, Japan;* [d]*Department of Immunobiology and Pharmacological Genetics, Graduate School of Medicine and Pharmaceutical Science for Research, University of Toyama, Toyama, Japan;* [e]*Prefectural Institute for Pharmaceutical Research, Toyama, Japan*

(Received 4 December 2007; revised 30 January 2008; accepted 7 February 2008)

Objective. **Various cytokines and growth factors control the differentiation and maturation of megakaryocytes (MKs). However, the mechanism regulating platelet release from MKs is not well understood. Here, we investigated a role of Lnk/Sh2b3, an intracellular adaptor protein, in megakaryopoiesis.**

Materials and Methods. **Number of MK progenitor in bone marrow (BM) of wild-type or *Lnk*$^{-/-}$ mice and their sensitivity to thrombopoietin (TPO) were determined in colony-forming unit assay. Using BM-derived wild-type or *Lnk*$^{-/-}$ MKs stimulated with TPO, activation of the signaling molecules was biochemically analyzed and effect of integrin stimulation on TPO signals was studied by addition of vascular cell adhesion molecule (VCAM-1). Platelet production from MKs in the presence of VCAM-1 was counted by flow cytometry and their morphological change was observed by time-lapse microscopy.**

Results. ***Lnk*$^{-/-}$ mice showed elevated platelets and mature MKs due to enhanced sensitivity of progenitors to TPO. Erk1/2 phosphorylation induced by TPO was augmented and prolonged in *Lnk*$^{-/-}$ MKs while activation of signal transducers and activators of transcription (Stat)3, Stat5, and Akt was normal. Wild-type MKs, but not in *Lnk*$^{-/-}$ MKs on VCAM-1 showed reduced Stat5 phosphorylation and mitogen-activated protein kinases activation upon stimulation with TPO. Additionally, the presence of VCAM in culture accelerated spontaneous platelet release from mature wild-type MKs, but not from *Lnk*$^{-/-}$ MKs.**

Conclusions. **Results suggest that contact of MKs with adhesion molecules via integrins might contribute to platelet release, which is under Lnk-mediated regulation of Stat-5 activation and show that Lnk functions in responses controlled by cell adhesion and in crosstalk between integrin- and cytokine-mediated signaling.** © **2008 ISEH - Society for Hematology and Stem Cells. Published by Elsevier Inc.**

Megakaryocytes (MKs) and the platelets they produce are required for normal thrombosis and hemostasis [1]. Recent evidence indicates early roles of platelets in innate immune responses and tumor cell biology [2]. MK progenitors that reside in the bone marrow (BM) undergo endomitosis and differentiate into large, MKs with polyploidy in preparation for platelet production [3]. Thousands of platelets can be released from a single MK into the bloodstream. Thrombopoietin (TPO) is required for both MK development and maintenance of platelet production. Mutant mice lacking TPO or its receptor, c-Mpl, show severe thrombocytopenia [4,5]. However, the remaining platelets in those mice are morphologically and functionally normal [6]. Thus, the TPO/c-Mpl system plays a critical role in the survival and proliferation of MKs, but is not indispensable for either MK maturation or release of platelets.

*H. Takizawa's present address is Institute for Research in Biomedicine, 6500 Bellinzona, Switzerland.

Offprint requests to: Satoshi Takaki, M.D., Ph.D., Research Institute, International Medical Center of Japan, 1-21-1 Toyama, Shinjuku-Ku, Tokyo 162-8655, Japan; E-mail: stakaki@ri.imcj.go.jp

0301-472X/08 $–see front matter. Copyright © 2008 ISEH - Society for Hematology and Stem Cells. Published by Elsevier Inc.
doi: 10.1016/j.exphem.2008.02.004

A critical step in thrombopoiesis is migration and adhesion of MKs to sinusoidal endothelial cells, where proplatelets elongate into the extravascular space [7–9]. The process is regulated by a variety of chemokines and cytokines as well as by adhesive interactions between adhesion molecules and extracellular matrix proteins. Mice lacking P-selectin, but not E-selectin, show increased numbers of interleukin (IL)-3–responsive MK progenitors and mature MKs with high ploidy [10]. A deficiency of platelet-endothelial cell adhesion molecule-1 leads to migration defects of MKs in response to stromal cell-derived factor-1 (SDF-1) and their increased adhesion to BM matrix proteins [11,12]. SDF-1 promotes localization of MK progenitors to the sinusoidal vascular zone in BM. This occurs through vascular cell adhesion molecule-1 (VCAM-1) and fibroblast growth factor-4 augmented very late antigen-4 (VLA-4)–mediated adhesion of MKs to endothelial cells, enhancing both MK survival and maturation [13]. These findings suggest pivotal roles of MK interaction with endothelial cells in BM via integrins and their ligands as well as cytokine-independent regulation in thrombopoiesis.

Lnk, recently designated as SH2B adaptor protein 3 (Sh2b3), belongs to an adaptor protein family composed of SH2-B (Sh2b1) and adaptor protein with PH and SH2 domains, APS (Sh2b2). Lnk negatively regulates lymphopoiesis and early hematopoiesis. *Lnk*-deficiency results in enhanced production of B cells partly due to enhanced signaling through c-Kit, and expansion as well as enhanced function of hematopoietic stem cells (HSCs) [14–16]. In addition, it appears that Lnk negatively controls erythropoietin- and TPO-dependent signals in erythropoiesis and thrombopoiesis [16–18]. Our previous study revealed that motility of hematopoietic progenitor cells on VCAM-1, an integrin ligand, was modulated by Lnk-mediated pathways [19]. Although the expansion of HSCs in $Lnk^{-/-}$ mice is largely TPO-dependent, it appears that the enhanced capability of $Lnk^{-/-}$ HSCs for repopulating irradiated host animals is not accomplished solely by a TPO-dependent pathway [20]. These observations suggest that Lnk might participate in control of integrin-mediated cell motility in addition to regulation of cytokine-dependent growth.

In this study, we investigated the possibility that Lnk might control thrombopoiesis by modulating integrin-mediated responses in addition to TPO-dependent growth signaling. Lnk specifically suppressed TPO-induced activation of Erk1/2, constraining the sensitivity of MKs to TPO. Costimulation of MKs with TPO and VCAM-1 resulted in downregulation of signal transducers and activators of transcription (Stat) 5 and upregulation of mitogen-activated protein kinase (MAPK) activation compared to stimulation by TPO alone. Those changes mediated by co-stimulation by TPO and VCAM-1 were not observed in MKs lacking Lnk. Our results revealed a formerly unrecognized regulatory mechanism in thrombopoiesis through integrin signaling and showed that Lnk modulates crosstalk between integrin-mediated signals and cytokine-induced signals.

Materials and methods

Mice and reagents

C57BL/6 mice were purchased from CLEA Japan (Tokyo, Japan). $Lnk^{-/-}$ mice [14–16] and green fluorescent protein (GFP) transgenic mice [21], both are on C57BL/6 background, were bred and maintained under specific pathogen-free conditions at the animal facility of the Institute of Medical Science, the University of Tokyo. Recombinant human TPO, mouse IL-3, and mouse IL-6 were purchased from Peprotech (London, UK). Mouse VCAM-1/Fc chimera was provided by R&D Systems (Minneapolis, MN, USA). Purified human fibrinogen was from American Diagnostica Inc. (Stamford, CT, USA). Human collagen type I was from Nycomed Pharma GmbH (Munich, Germany). Anti–β-actin (clone 2.1) was obtained from Sigma (St. Louis, MO, USA), while anti–phospho-Stat5 (pTyr694), anti–phospho-Stat3 (pTyr705), anti-Stat3, anti–phospho-Akt (Ser473), anti-Akt, anti–phospho-Erk1/2 (pThr202/pTyr204), anti-Erk1/2, anti–phospho-p38 (pThr180/pTyr182), and anti-p38 were purchased from Cell Signaling Technology (Danvers, MA, USA). Additional antibodies included anti-Stat5a and anti-Stat5b (Santa Cruz Biotechnologies Inc., Santa Cruz, CA, USA), and secondary antibodies, horseradish peroxidase–coupled goat anti-rabbit IgG and sheep anti-mouse IgG (Amersham Pharmacia Biotechnology). Anti-Lnk antibodies were generated [14,15].

Flow cytometric analysis

BM cells or splenocytes from wild-type and Lnk-deficient mice were harvested with Iscove's modified Eagle's medium (IMDM; GIBCO, Invitrogen, Grand Island, NY, USA) containing 2% fetal bovine serum (FBS), incubated with anti-FcRγ2 antibody (2.4G2) to block nonspecific binding and stained with fluorescein isothiocyanate or phycoerythrin-conjugated anti-CD41 (MWReg30; BD Biosciences, San Jose, CA, USA). The percentage of $CD41^+$ cells in total BM was determined with a FACSCalibur instrument (BD Biosciences), and the absolute number of $CD41^+$ MKs in BM or spleen was calculated. The ratio of GFP^+ platelets in total $CD41^+$ platelets was also determined by flow cytometry. For polyploidy analysis, BM cells directly harvested from wild-type and $Lnk^{-/-}$ mice were dissociated in CATCH buffer (Hank's balanced salt solution [GIBCO, Invitrogen], including 0.38% sodium citrate, 1 mM adenosine, and 2 mM theophylline) and stained with fluorescein isothiocyanate-CD41 antibody. To stain nuclei, the labeled cells were washed and incubated overnight in 100 μg/mL propidium citrate and 50 μg/mL RNase in 1% sodium citrate solution at 4°C and subjected to flow cytometric analysis. For MKs used in the following biochemical analysis and in vitro platelet formation, bone marrow cells were cultured for 3 days and the ploidies of MKs purified from the culture were analyzed by the same method as described.

Platelet count

Peripheral blood was taken from wild-type and Lnk-deficient mice retro-orbitally and platelet count was analyzed on the flow cytometer programmed with mouse-specific parameter (Sysmex, Hyogo, Japan).

In vivo turnover of platelets

Platelet-rich plasma from GFP transgenic mice or GFP transgenic $Lnk^{-/-}$ mice was separated by centrifugation of whole blood at 150*g* for 15 minutes without braking. One micrometer prostaglandin E_1 and 5 U/mL apyrase (Sigma) were added followed by centrifugation at 750*g* for 10 minutes. The platelet pellet was resuspended in modified Tyrode-HEPES buffer pH 7.4 (10 mM HEPES, 12 mM $NaHCO_3$, 138 mM NaCl, 5.5 mM glucose, 2.9 mM KCl, and 1 mM $MgCl_2$) and the concentration was determined on the flow cytometer (Sysmex). Resultant platelets (2.5×10^9) were intravenously injected into wild-type C57BL/6 mice or $Lnk^{-/-}$ mice. Peripheral blood was collected by plastic tip from the retro-orbital sinus of recipient mice at several time points and was incubated with biotinylated anti-CD41 and peridinin-chlorophyll-protein–conjugated streptavidin for 20 minutes at room temperature, and the percentage of GFP^+ platelets was determined on a FACSCalibur.

Immunohistochemistry

Freshly dissected nondecalcified femurs from 6- to 8-week-old wild-type C57BL/6 mice or $Lnk^{-/-}$ mice were embedded in 4% carboxymethyl cellulose (FINETEC, Fuchu, Japan) and snap-frozen in N-hexane chilled in a slurry of ethanol and dry ice. Sections were generated via Kawamoto's film method (Cryofilm transfer kit; FINETEC). The 150-μm–thick cryostat sections were first blocked with 5% FBS/phosphate-buffered saline and then stained with fluorescein isothiocyanate–conjugated anti-CD41 in blocking buffer. Cell nuclei were labeled with TO-PRO3 (Molecular Probes, Invitrogen). Sections were then mounted with PERMAFLUOR (Beckman Coulter, Fullerton, CO, USA), and confocal microscopic analysis was performed with an Olympus FV-500 confocal microscope.

In vitro colony assays

BM cells were flushed from femurs of wild-type or $Lnk^{-/-}$ mice with IMDM (GIBCO, Invitrogen) containing 2% FBS. Marrow cells (1×10^5) were cultured in double-chamber slides using MegaCult-C (Stem Cell Technologies, Vancouver, Canada) in the presence of different concentration (0, 0.1, 1, 10, and 100 ng/mL) of human TPO or 100 ng/mL TPO, 10 ng/mL mouse IL-3, and 20 ng/mL mouse IL-6. After 7 days of cultivation, slides were dehydrated in cold acetone for 5 minutes and colonies were stained for acetylcholinesterase activity with 5 mM sodium citrate solution, including 3 mM $CuSO_4$, 0.5 mM $K_3[Fe(CN)_6]$, and 75 mM Na_2HPO_4 (pH 6.0). Slides were scored microscopically, and megakaryocyte colonies were defined as colonies with at least three megakaryocytes.

Megakaryocyte culture and purification

Lineage-negative BM cells (depleted of cells expressing B220, CD3, Mac-1, Gr-1, and TER-119) were enriched using Hematopoietic Progenitor Cell Enrichment Set (BD Bioscience) following manufacturer's protocol. In brief, BM cells were labeled with a biotinylated cocktail of lineage-specific antibodies followed by Streptavidin-conjugated magnetic beads and lineage marker–negative (Lin^-) cells were collected using BD IMagnet. Lin^- cells (1×10^6) were incubated in IMDM containing 0.5% bovine serum albumin (BSA), 10 ng/mL human transferrin, human insulin, 1.6 μg/mL low density lipoprotein, 40 μM adenosine triphosphate, 40 μM uridine triphosphate, 40 μM cytidine triphosphate, 40 μM guanosine triphosphate (Sigma), 50 μM 2-mercaptoethanol, 29.2 μg/mL L-glutamine, 100 IU/mL penicillin, and 100 μg/mL streptomycin (GIBCO, Invitrogen), in the presence of 20 ng/mL or 2 ng/mL TPO for wild-type or $Lnk^{-/-}$ cells, respectively. After culturing for 3 days, mature MKs were harvested by low-speed centrifugation (120*g* for 10 minutes) and purified by gravity sedimentation through discontinuous BSA (0%/1.5%/3%) for 45 minutes at room temperature.

Immunoblotting

Purified mature MKs after 3-day cultivation were washed with IMDM and further incubated in the absence of TPO for 16 hours for starvation. Subsequently, cells were stimulated with 10 ng/mL TPO for 0, 10, 30, and 60 minutes, and lysed in RIPA buffer (0.1% sodium dodecyl sulfate, 1% Triton X-100, 1% sodium deoxycholate, 158 mM NaCl, 10 mM Tris-HCl, 1 mM ethylene glycol tetraacetic acid, 5 mM ethylene diamine tetraacetic acid, 100 U/mL aprotinin, 1 mM sodium vanadate, 10 mM sodium fluoride, 10 μg/mL leupeptin, and 2 mM phenylmethylsulfonyl fluoride). For integrin stimulation experiments, purified and starved MKs were stimulated with 10 ng/mL TPO and 50 μg/mL VCAM-1, fibrinogen or collagen type 1 in the presence of 2 mM manganese for 10 minutes and lysed. Thirty-five micrograms of total protein was subjected to immunoprecipitation and immunoblotting using anti-Lnk antibodies or other antibodies as described previously [14].

In vitro platelet formation

Twenty-four–well plates were precoated with 20 μg/mL mouse recombinant VCAM-1 overnight at 4°C and washed three times with MK-conditioned media. Purified mature MKs as described above were incubated on BSA- or VCAM-1–coated plates including 250 μL the conditioned media including 1 ng/mL TPO for 12 hours, and the culture supernatant was collected after addition of ethylene diamine tetraacetic acid at a final concentration of 10 mM. Flow-Count Fluorospheres (Beckman Coulter) were added and platelets gated on the same scatter properties as freshly prepared blood platelets were enumerated with a flow cytometer. For anti-integrin-α4 antibody treatment, purified cells were incubated with anti-CD49d, the α4 chain of the VLA-4 (PS/2; SouthernBiotech, Birmingham, AL, USA) at the concentration of 10 μg/mL for 30 minutes prior to the assay.

Proplatelet formation analysis

Harvested fetal liver cells (E13 to 15) were incubated in DMEM including 10% FBS, 100 IU/mL penicillin, 100 μg/mL streptomycin, and 29.2 μg/mL L-glutamine, in the presence of 20 ng/mL or 2 ng/mL TPO for wild-type or $Lnk^{-/-}$ cells. After 3 to 5 days of cultivation, mature MKs were purified as described and washed with Leibovitz's L-15 medium (GIBCO, Invitrogen). MKs in suspension were mounted in semi-solid medium including 20% Leibovitz's L-15, 80% MegaCult M-3234 (Stem Cell Technologies) and 1 ng/mL TPO in 35-mm Petri dishes with a 10-mm glass hole (Matsunami Glass, Osaka, Japan) coated with 10 μg/mL BSA or VCAM-1. Images of proplatelet formation were obtained using confocal microscopy in a CO_2 chamber (FV500; Olympus, Tokyo, Japan).

Results

Mature platelets are increased in the absence of Lnk, but showed normal turnover in circulation

Platelets develop from HSCs in the BM. HSCs give rise to multipotent progenitors, differentiate into committed MK progenitors, and then further proliferate and differentiate into mature MKs. Platelets released from mature MKs circulate throughout the body for several days, and are eventually captured and degraded by macrophages in the spleen and liver. TPO plays key roles in the proliferation and maturation of MK progenitors and megakaryocytes, as well as in the expansion of HSCs. Previous studies by this and other groups have demonstrated that Lnk negatively regulates TPO-dependent signals in megakaryocytic cells as well as in HSCs [17,20,22]. Velazquez et al. reported deregulated hematopoiesis including thrombocytosis in *Lnk*-deficient mice [16]. Furthermore, Tong et al. showed that various signaling molecules downstream of c-Mpl (the TPO receptor), such as Jak2 tyrosine kinase, Stat-5, Erk1/2, and Akt are all hyperactivated in *Lnk*-deficient MK progenitors [17].

We attempted to confirm those observations, and also to define the steps in thrombopoiesis, which were regulated by Lnk-dependent pathway(s). First, we examined expression of Lnk protein in MK-lineage cells, and found that substantial amounts of Lnk protein were expressed in MKs and maintained by mature platelets (Fig. 1A, and data not shown). The number of platelets in peripheral blood was increased nearly fivefold in *Lnk*-deficient mice compared with normal mice (Fig. 1B), consistent with previous observations by Velazquez et al. The absence of Lnk in mature platelets might change their survival and turnover rate in circulation. We assessed the half-life of platelets and the phagocytic function of macrophages by adoptive transfer. Platelet-rich fractions were prepared from the blood of GFP-transgenic mice or GFP-transgenic $Lnk^{-/-}$ mice, and transferred into *Lnk*-sufficient normal mice (Fig. 1C) or *Lnk*-deficient mice (Fig. 1D). In both conditions, transferred *Lnk*-deficient platelets disappeared from peripheral blood at almost the same rate as normal mature platelets. The survival of mature platelets in circulation as well as removal and degradation of old platelets by peripheral macrophages were not affected by the absence of Lnk.

Increased MK precursors in $Lnk^{-/-}$ mice and their distribution in BM

Next, we examined thrombopoiesis in the BM. $CD41^+$ MKs were significantly increased threefold in BM and nearly tenfold in the spleen (Fig. 2A). To determine whether MKs accumulated within specific regions of the BM of $Lnk^{-/-}$ mice, we undertook an immunohistochemical analysis. As shown in Figure 2B, numerous $CD41^+$ MKs were diffusely present throughout the BM in the femur in $Lnk^{-/-}$ mice, and no particular accumulating spot of $CD41^+$ cells was observed.

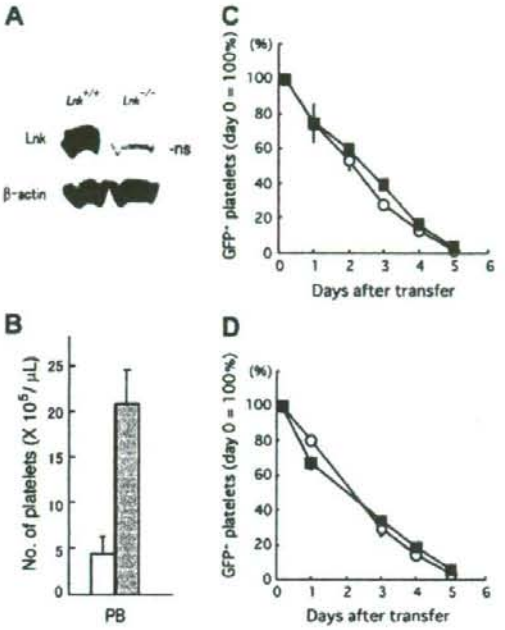

Figure 1. Lnk expression in megakaryocytes (MKs) and thrombocytosis in Lnk-deficient mice. (**A**) Substantial expression of Lnk in MKs. Lin^- cells obtained from bone marrow (BM) of $Lnk^{+/+}$ or $Lnk^{-/-}$ mice were cultured in the presence of 20 ng/mL or 2 ng/mL thrombopoietin (TPO), respectively. After a 3-day incubation, mature MKs were purified on density gradients and lysed. Total proteins were separated and immunoblotted with an anti-Lnk antibody (upper panel) or with an anti-actin antibody, as loading control (lower panel). NS = nonspecific band. (**B**) Fivefold increase in number of platelets in $Lnk^{-/-}$ mice. Peripheral blood was obtained retro-orbitally from $Lnk^{+/+}$ (open column) or $Lnk^{-/-}$ (closed column) mice and platelet counts were measured by flow cytometry. (**C, D**) Platelet turnover in $Lnk^{-/-}$ mice. Platelets obtained from green fluorescent protein-positive (GFP^+) wild-type (open circle) or GFP^+ $Lnk^{-/-}$ (closed square) mice were transferred to $Lnk^{+/+}$ (**C**) or $Lnk^{-/-}$ mice (**D**). Peripheral blood was taken from the recipient mice and the percentage of GFP^+ platelets was determined by flow cytometry. The relative percentage of GFP^+ platelets was calculated by dividing the percentage of GFP^+ platelets at each indicated time point by that at the day of transfer (Day 0).

$Lnk^{-/-}$ MK precursors are hypersensitive to TPO and hypermature

The increase in MKs may be due to increased proliferation of progenitors and/or prolonged survival and maturation of MKs. Growth of MK progenitors and their sensitivity to TPO were evaluated by colony-forming assays. $Lnk^{-/-}$ progenitors formed colonies even at very low concentrations of TPO whereas normal progenitors hardly responded. Furthermore, the number of colony-forming cells upon full stimulation with TPO, IL-6, and IL-3 was twofold higher in $Lnk^{-/-}$ BM than in wild-type (Fig. 3A). Maturation of

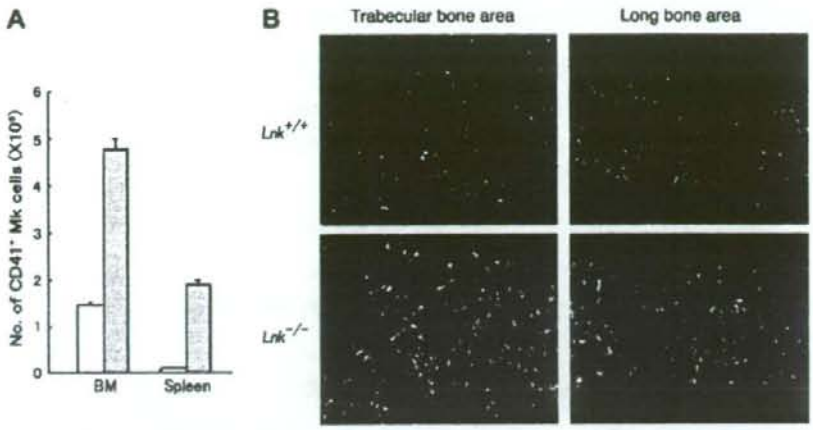

Figure 2. Megakaryocytes (MKs) numbers are increased in bone marrow (BM) and spleen of $Lnk^{-/-}$ mice. (**A**) Significant increase in MKs in BM and spleen. BM cells (left panel) or splenocytes (right panel) were harvested from $Lnk^{+/+}$ (open column) or $Lnk^{-/-}$ (closed column) mice and the percentage of $CD41^+$ MKs was determined by flow cytometry. The absolute number of $CD41^+$ MKs in each tissue was calculated by multiplying the percentage by the absolute number of total mononuclear cells. Shown are mean ± SD of results obtained from two experiments. (**B**) Immunofluorescence microscopic analysis of $Lnk^{-/-}$ BM. Frozen sections of femurs from $Lnk^{+/+}$ (upper) or $Lnk^{-/-}$ (lower) mice were stained with anti-CD41 (green) and TO-PRO3 (blue) and observed in confocal microscopy. Representative images of trabecular bone (left column) and long bone regions (right column) are shown.

MKs in BM also was quantified by measuring their ploidies. Polyploidy analysis of MKs in BM using flow cytometry showed that mature MKs with high polyploidy (32N and 64N) were more frequent in $Lnk^{-/-}$ BM. In contrast, a majority of MKs in normal BM had 16 nuclei (Fig. 3B). These data indicate that Lnk regulates the proliferation of MK progenitors by limiting their sensitivity to TPO, and *Lnk*-deficiency promoted expansion of MK-lineage cells. It seemed that Lnk also played a role in controlling maturation of MKs.

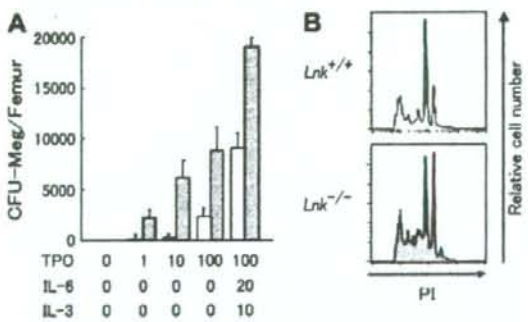

Figure 3. Megakaryocytosis in $Lnk^{-/-}$ mice. (**A**) Increased number of megakaryocytes (MK) progenitors and their hypersensitivity to thrombopoietin (TPO). Total bone marrow (BM) cells obtained from the BM of $Lnk^{+/+}$ (open column) or $Lnk^{-/-}$ (closed column) mice were cultured at the indicated concentration of TPO, interleukin (IL)-3, and IL-6 for 7 days. The mean ± SD of the number of colonies per femur are shown from three independent experiments. (**B**) BM cells of $Lnk^{+/+}$ (upper column) or $Lnk^{-/-}$ (lower column) mice were analyzed for DNA content. Representative data of multiple experiments are shown.

Lnk-deficiency causes augmented MAPK activation in MKs upon stimulation with TPO

To understand the molecular mechanism by which Lnk regulates TPO-induced MK proliferation, we examined overall protein phosphorylation following TPO stimulation using BM-derived MKs. We generated MKs with the same ploidy from wild-type and $Lnk^{-/-}$ mice by adjusting TPO concentration to levels that induced relatively comparable proliferative responses, and used them for biochemical analyses (Fig. 4A). Purified MKs were starved for 16 hours in TPO-free medium, stimulated with 10 ng/mL TPO and then lysed at several time points. The cell lysates were subjected to immunoblotting analyses for signaling molecules activated and phosphorylated downstream of c-Mpl (Fig. 4B). Stat3 and Akt was phosphorylated ten minutes after TPO stimulation and lasted >60 minutes in wild-type cells. Activation of Stat5, p38, and Erk1/2 was transiently observed, with peak phosphorylation 10 minutes after TPO stimulation. In $Lnk^{-/-}$ MKs, Erk1/2 activation was prolonged while phosphorylation levels of the other signaling molecules were essentially comparable to those induced in wild-type cells. Thus, our results indicated that Lnk specifically inhibited activation or regulates inactivation of Erk1/2 in TPO-dependent (c-Mpl–mediated) signaling pathways in MKs.

Megakaryocytic responses to combined exposure to TPO and integrins are modulated by expression of Lnk

Our previous study showed that the motility of hematopoietic progenitor cells on VCAM-1 was regulated by Lnk-mediated pathways [19]. We, therefore, asked whether

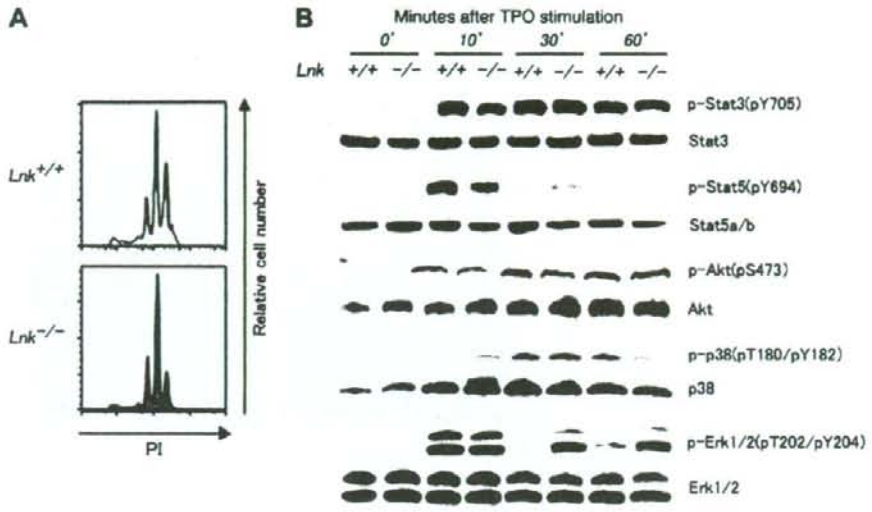

Figure 4. Thrombopoietin (TPO)-mediated hyperactivation of Erk1/2 in $Lnk^{-/-}$ megakaryocytes (MKs). (**A**) Equivalent ploidy between $Lnk^{+/+}$ and $Lnk^{-/-}$ MKs. Lin^- populations harvested from $Lnk^{+/+}$ (upper column) or $Lnk^{-/-}$ (lower column) mice were cultured in the presence of 20 ng/mL or 2 ng/mL TPO, respectively. (**B**) Augmented phosphorylation of Erk1/2 in Lnk-deficiency. Purified mature MKs were starved for 16 hours in the absence of TPO and re-stimulated with 10 ng/mL TPO for the indicated period. Total cell lysates were subjected to immunoblotting using indicated antibodies. Typical results of three independent experiments are shown.

additional stimuli through integrins might affect TPO-mediated megakaryopoiesis. It was also important to determine whether Lnk might be involved in integrin-mediated signaling pathways in MKs. Phosphorylation of cellular proteins was examined in both wild-type and $Lnk^{-/-}$ MKs, which were exposed to VCAM-1 in the presence of TPO and manganese to activate integrins. In wild-type cells, costimulation with TPO and VCAM-1 significantly inhibited Stat5 phosphorylation, and enhanced activation of p38 and Erk1/2 (Fig. 5A). On the other hand, in $Lnk^{-/-}$ MKs, TPO-dependent Stat5 activation was clearly induced even in the presence of VCAM-1 costimulation, while p38 activation was not enhanced (Fig. 5A). These observations suggest that costimulation by integrin engagement changed the nature of signals downstream of c-Mpl in MKs. Downregulated activation of Stat5 by VCAM-1 as well as augmented activation of p38 and Erk1/2 by VCAM-1 seemed to require Lnk-mediated pathways.

Costimulation by VCAM-1 and TPO reduces the release of platelets by $Lnk^{-/-}$ MKs

VCAM-1 is a ligand for α4β1 and α4β7 integrins and is expressed mainly on endothelial cells [23,24]. Adhesive interaction between endothelial cells and MKs through the VLA-4/VCAM-1 axis promotes maturation of megakaryocytes [25]. To examine how VCAM-1–mediated changes in TPO-induced cellular responses affected certain MK functions, we evaluated platelet release from mature MKs in vitro. Purified MKs were incubated on BSA- or VCAM-1–coated plates for 12 hours, after which the number of released platelets was counted by flow cytometry. In the absence of TPO, wild-type and $Lnk^{-/-}$ MKs produced similar numbers of platelets on BSA- and VCAM-1–coated plates. In the presence of TPO, wild-type MKs on VCAM-1 released greater numbers of platelets than those on BSA. In contrast, the number of platelets released by TPO-stimulated $Lnk^{-/-}$ cells on VCAM-1 was comparable to that observed with BSA. The number of released platelets from $Lnk^{-/-}$ MKs was significantly lower than that from normal cells on VCAM-1 (Fig. 5B and Table 1). Pretreatment by anti-integrin-α4 antibody completely abolished the difference in platelet production between $Lnk^{-/-}$ and wild-type cells on VCAM-1 (Fig. 5B). Apoptosis of MKs leads to generation of functional platelets [26]. There was, however, no difference in the percentage of apoptotic cells or their ploidy between wild type and $Lnk^{-/-}$ cells either on BSA- or VCAM-1–coated plate (data not shown).

We examined the possibility that reduced platelet formation by $Lnk^{-/-}$ MKs on VCAM was due to morphological changes in MKs. We generated proplatelet-forming MKs from wild-type and $Lnk^{-/-}$ fetal liver progenitors and monitored their morphological changes on BSA and VCAM-1 by time-lapse confocal microscopic analysis (Fig. 6). While the wild-type MKs elongated proplatelets with pseudopodia shape on BSA, they produced more branched proplatelets from firmly attached and well-expanded cell body on VCAM-1. $Lnk^{-/-}$ MKs on BSA showed proplatelet formation comparable to that of wild-type cells on BSA.

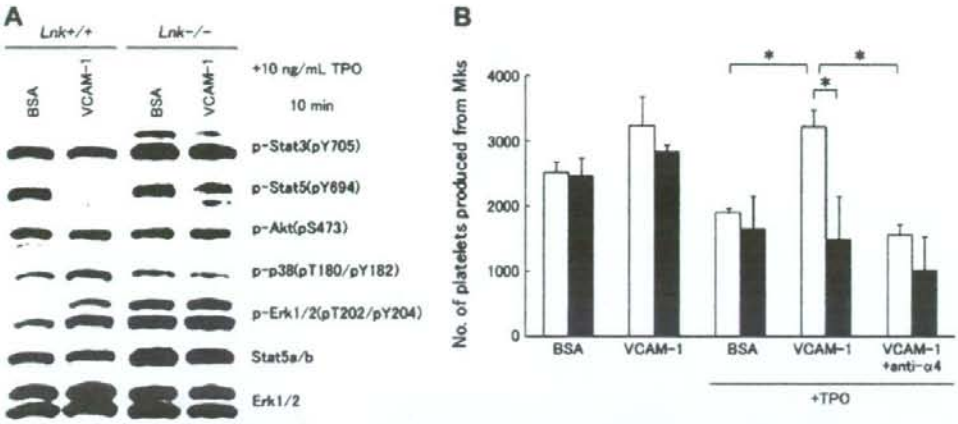

Figure 5. Changes of thrombopoietin (TPO)-induced cellular response by integrin ligands. (**A**) Modulation of TPO signaling pathways by integrin ligands. Mature megakaryocytes (MKs) obtained from $Lnk^{+/+}$ or $Lnk^{-/-}$ mice were starved for 16 hours without TPO and restimulated with both 10 ng/mL TPO and 50 μg/mL of vascular cell adhesion molecule-1 (VCAM-1). After 10 minutes incubation, cells were lysed and the lysates subjected to immunoblotting using the indicated antibodies. Results of several experiments are shown. (**B**) Augmented platelet production in the presence of VCAM-1. Purified $Lnk^{+/+}$ (open column) or $Lnk^{-/-}$ (closed column) MKs were incubated on either 20 μg/mL bovine serum albumin (BSA)- or VCAM-1–coated plates with or without addition of 1 ng/mL TPO for 12 hours. For anti-integrin-α4 antibody treatment, cells were preincubated with 10 μg/mL anti-CD49d for 30 minutes prior. The number of platelets was measured by flow cytometry. Shown are mean ± SD of results obtained from three independent experiments. *$p < 0.01$ comparison of $Lnk^{+/+}$ cells on VCAM-1–coated plates with that of $Lnk^{+/+}$ cells on BSA-coated plates, of $Lnk^{-/-}$ cells on VCAM-1–coated plates and of antibody-treated $Lnk^{+/+}$ cells on VCAM-1–coated plates.

However, $Lnk^{-/-}$ MKs on VCAM-1 developed proplatelets from not only the edge but also the center of the cell body with enlarged pseudopodial ends. This result suggests that a stimulation of integrin bound to VCAM-1 promoted platelet production by forming more proplatelets in wild-type MKs, and Lnk plays a role in regulating morphological changes for proplatelet formation.

Discussion

In this study, we demonstrated that $Lnk^{-/-}$ MK progenitors were hypersensitive to TPO, causing increased MK numbers, hypermaturation, and delayed platelet production on VCAM-1, which in turn led to thrombocytosis. It has been previously reported that *Lnk*-deficiency resulted in hyperactivation of TPO-dependent signaling molecules including Stat3, Stat5, Akt and Erk1/2 in MKs [17]. We also observed a significant enhancement in TPO-induced activation of Erk1/2 in $Lnk^{-/-}$ MKs, but not Stat3, Stat5 nor Akt in our experimental settings. The reasons for the discrepancy are currently unknown, but might be ascribed to the differences in the preparation of MKs used for biochemical analysis. Because the sensitivity of MKs to TPO declines during maturation and increase in ploidy [27], we prepared wild-type and $Lnk^{-/-}$ MKs with equalized ploidy and high purity from cultivated BM cells. MKs isolated by flow cytometric sorting from normal and *Lnk*-deficient mice might have different ploidy and purity because of low frequency and fragility of MKs in BM. Enhanced responses against other cytokines that activate Jak/Stat pathway, such as IL-3 or IL-7, have been suggested in the absence of Lnk. However, we did not observe any enhancements of cellular responses by IL-3, IL-7, and IL-5 in $Lnk^{-/-}$ precursors ([14,22] and unpublished observations). We believe that the inhibition of TPO-induced signals by

Table 1. VCAM-1 increases platelet release by megakaryocytes in the presence of Lnk

	Platelet production ratios in the presence of VCAM-1[a]	
	Genotype	
Cytokine addition	$Lnk^{+/+}$	$Lnk^{-/-}$
–TPO	1.19 ± 0.07	1.05 ± 0.18
+TPO	1.86 ± 0.15*	1.25 ± 0.27**

[a]Lin$^-$ bone marrow (BM) precursor cells from wild-type or $Lnk^{-/-}$ mice were incubated for 3 days in the presence of 20 ng/mL or 2 ng/mL thrombopoietin (TPO), respectively. Purified megakaryocytes were incubated with or without 1 ng/mL TPO for an additional 12 hours. The number of platelets released in culture on vascular cell adhesion molecule (VCAM-1)–coated plates was counted by flow cytometry and compared with that on bovine serum albumin (BSA)–coated plates (see also Fig. 5B). Platelet production ratios were calculated by dividing the number of platelets on VCAM-1–coated membranes by that on BSA-coated membranes in the absence or presence of TPO. Data are presented as mean ± SD of results from three independent experiments.

*$p < 0.003$ compared with that of $Lnk^{-/-}$ in the presence of TPO or that of $Lnk^{+/+}$ in the absence of TPO.

**$p > 0.2$ compared with that of $Lnk^{-/-}$ in the absence of TPO.

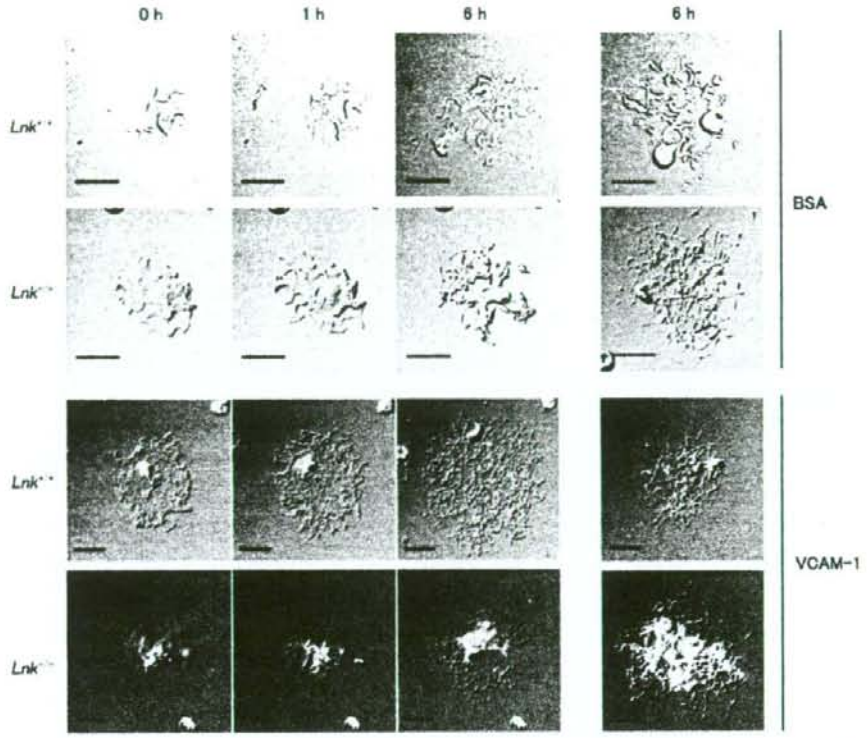

Figure 6. Morphological changes of $Lnk^{-/-}$ megakaryoctyes (MKs) producing proplatelets on vascular cell adhesion molecule-1 (VCAM-1). Fetal liver–derived $Lnk^{+/+}$ or $Lnk^{-/-}$ MKs were cultured on bovine serum albumin (BSA)– (upper panels) or VCAM-1–coated plates (lower panels) in microscope chambers and images were taken every hour up to 24 hours. Shown are representative images taken at the beginning of proplatelet elongation (0 hours), and following 3- and 6-hour observation. Images of another independent MKs at 6 hours were also shown. Scale bars: 50 μm.

Lnk involves cellular machinery specific to c-Mpl and does not act via Jak2 activation.

Our results revealed novel regulatory mechanisms in thrombopoiesis mediated by Lnk in addition to its role in constraining TPO signals. Additional stimulation by integrin ligand modulated TPO-induced signal responses of MKs. Engagement of integrin ligand induced strong mitogenic responses in MKs as well as in fibroblasts [28,29]. Interestingly, costimulation by TPO and VCAM-1 led to suppression of Stat5 phosphorylation and upregulation of p38 and Erk1/2 activation, which might change the nature of TPO-induced signals from ones supporting cell growth to those inducing cell-cycle arrest and differentiation. Consistently with this, we showed that normal MKs released greater numbers of platelets on VCAM-1 than on BSA. Administration of SDF-1 and fibroblast growth factor-4 to mice facilitates both MK maturation and platelet production by enhancing migration and adhesion of MK progenitors to BM endothelial cells through adhesion molecules including VCAM-1/VLA-4 [13]. Cellular interaction through VCAM-1 might trigger MKs to release platelets into the blood stream by terminating expression of Stat5-inducible genes after attachment of MKs to sinusoidal endothelial cells (Fig. 7A).

Inactivation of Stat5 was not observed in $Lnk^{-/-}$ MKs treated with TPO and VCAM-1. Additionally, platelet production from $Lnk^{-/-}$ MKs was not increased in the presence of VCAM-1. $Lnk^{-/-}$ MKs on VCAM-1 showed some morphological changes in proplatelet formation, which might be due to insufficient activation of demarcation membrane system of MKs [30], leading to inefficient platelet release in vitro upon integrin ligation by VCAM-1. In the absence of Lnk, MKs might continue undergoing endomitosis without producing platelets due to impaired Stat5 inactivation even if they contacted endothelial cells. This may lead to their hypermaturation in BM and result in more platelets production (Fig. 7B), because MKs with high ploidy are able to produce more platelets than those with low ploidy [31]. Thrombocytosis in $Lnk^{-/-}$ mice might be a consequence of increased numbers of MKs due to hypersensitivity of MK progenitors (TPO-dependent), in combination with accumulation of hypermature MKs attached

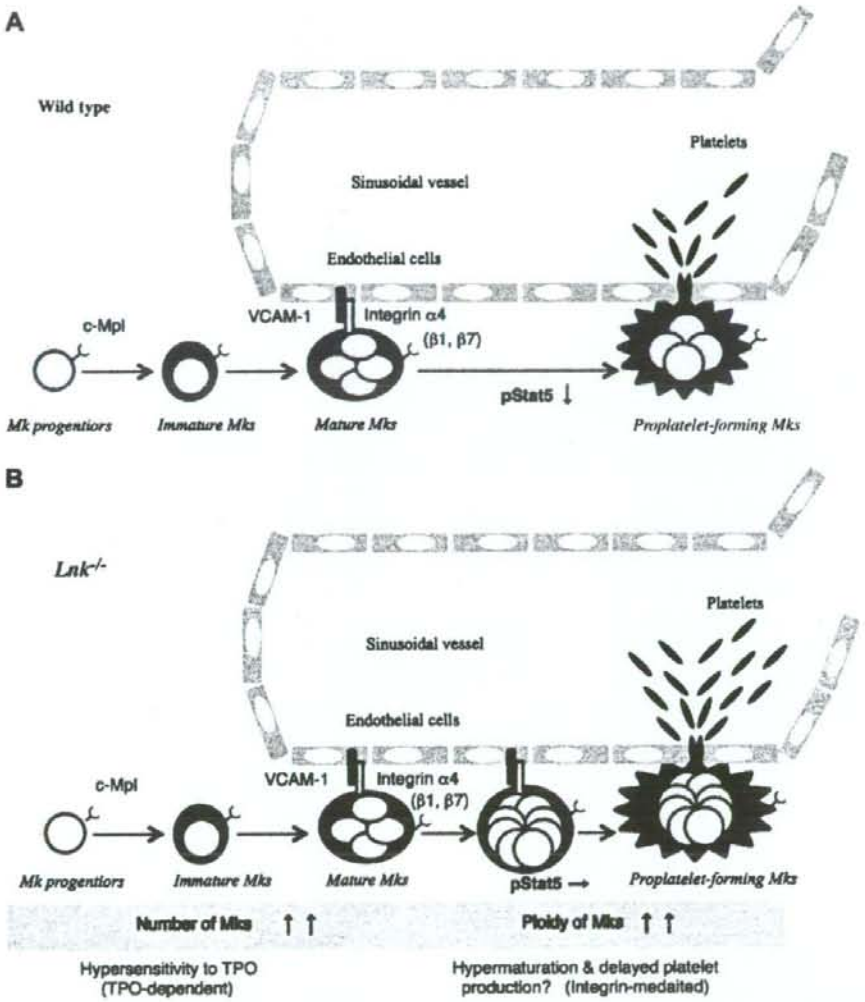

Figure 7. (A) Wild-type megakaryocytes (MK) progenitors proliferate and differentiate into mature MKs in response to thrombopoietin (TPO). When they contact the endothelial cells forming the sinusoidal vessels in bone marrow (BM) though integrinα4–vascular cell adhesion molecule-1 (VCAM-1) axis, platelets are released into bloodstream through proplatelet formation, which is possibly triggered by reduction of TPO-induced signal transducers and activators of transcription 5 (Stat5) activity upon VCAM-1 stimulation. (B) In the case of Lnk-deficiency, the number of mature MKs is increased due to enhanced sensitivity of $Lnk^{-/-}$ MK progenitor to TPO (TPO-dependent). After attaching the endothelial cell, MKs might keep undergoing endomitosis without platelet release, possibly due to impaired Stat5 inactivation, leading to their hypermaturation with an increase of ploidy.

to endothelial cells due to delayed platelet release (integrin-mediated) in Figure 7B. Future experiments will determine whether regulation of Stat5 is directly involved in initiation of platelet release, and how activation of Stat5 and MAPK in TPO-stimulated MKs is regulated by integrin- and Lnk-mediated events.

In summary, our results shed light on formerly unrecognized regulatory mechanisms in thrombopoiesis mediated by Lnk, and crosstalk between cytokines and integrins in MKs. TPO-induced Erk1/2 phosphorylation, but not activation of Stats and Akt, was constrained by Lnk, and was augmented in the absence of Lnk. Reduction of TPO-induced Stat5 and MAPKs activation in the presence of VCAM-1 co-ligation was mediated by a Lnk-dependent manner. Adhesion molecules play important roles in the biological properties of hematopoietic cells as environmental factors that determine cell fate. Understanding how integrin-mediated signals affect gene regulation or cytokine- or growth

factor–induced signaling pathways will be important to efforts to fully understand thrombopoiesis, hematopoiesis, and cellular responses.

Acknowledgments

We are grateful to our colleagues for helpful discussions, technical advices, and critical reading of this article. This work was supported by Grants-in-Aids from the Ministry of Education, Culture, Sports, Science and Technology, the Japanese Government. H.T is supported by Research Fellowship of the Japanese Society for the Promotion of Science for Young Scientists.

References

1. Kaushansky K. The molecular mechanisms that control thrombopoiesis. J Clin Invest. 2005;115:3339–3347.
2. Gupta GP, Massague J. Platelets and metastasis revisited: a novel fatty link. J Clin Invest. 2004;114:1691–1693.
3. Zimmet J, Ravid K. Polyploidy: occurrence in nature, mechanisms, and significance for the megakaryocyte-platelet system. Exp Hematol. 2000;28:3–16.
4. Gurney AL, Carver-Moore K, de Sauvage FJ, Moore MW. Thrombocytopenia in c-mpl-deficient mice. Science. 1994;265:1445–1447.
5. de Sauvage FJ, Carver-Moore K, Luoh SM, et al. Physiological regulation of early and late stages of megakaryocytopoiesis by thrombopoietin. J Exp Med. 1996;183:651–656.
6. Bunting S, Widmer R, Lipari T, et al. Normal platelets and megakaryocytes are produced in vivo in the absence of thrombopoietin. Blood. 1997;90:3423–3429.
7. Tavassoli M, Aoki M. Localization of megakaryocytes in the bone marrow. Blood Cells. 1989;15:3–14.
8. Zucker-Franklin D, Philipp CS. Platelet production in the pulmonary capillary bed: new ultrastructural evidence for an old concept. Am J Pathol. 2000;157:69–74.
9. Junt T, Schulze H, Chen Z, et al. Dynamic visualization of thrombopoiesis within bone marrow. Science. 2007;317:1767–1770.
10. Banu N, Avraham S, Avraham HK. P-selectin, and not E-selectin, negatively regulates murine megakaryocytopoiesis. J Immunol. 2002;169:4579–4585.
11. Dhanjal TS, Pendaries C, Ross EA, et al. A novel role for PECAM-1 in megakaryocytokinesis and recovery of platelet counts in thrombocytopenic mice. Blood. 2007;109:4237–4244.
12. Wu Y, Welte T, Michaud M, Madri JA. PECAM-1: a multifaceted regulator of megakaryocytopoiesis. Blood. 2007;110:851–859.
13. Avecilla ST, Hattori K, Heissig B, et al. Chemokine-mediated interaction of hematopoietic progenitors with the bone marrow vascular niche is required for thrombopoiesis. Nat Med. 2004;10:64–71.
14. Takaki S, Morita H, Tezuka Y, Takatsu K. Enhanced hematopoiesis by hematopoietic progenitor cells lacking intracellular adaptor protein. Lnk. J Exp Med. 2002;195:151–160.
15. Takaki S, Sauer K, Iritani BM, et al. Control of B cell production by the adaptor protein lnk. Definition of a conserved family of signal-modulating proteins. Immunity. 2000;13:599–609.
16. Velazquez L, Cheng AM, Fleming HE, et al. Cytokine signaling and hematopoietic homeostasis are disrupted in Lnk-deficient mice. J Exp Med. 2002;195:1599–1611.
17. Tong W, Lodish HF. Lnk inhibits Tpo-mpl signaling and Tpo-mediated megakaryocytopoiesis. J Exp Med. 2004;200:569–580.
18. Tong W, Zhang J, Lodish HF. Lnk inhibits erythropoiesis and Epo-dependent JAK2 activation and downstream signaling pathways. Blood. 2005;105:4604–4612.
19. Takizawa H, Kubo-Akashi C, Nobuhisa I, et al. Enhanced engraftment of hematopoietic stem/progenitor cells by the transient inhibition of an adaptor protein. Lnk. Blood. 2006;107:2968–2975.
20. Buza-Vidas N, Antonchuk J, Qian H, et al. Cytokines regulate postnatal hematopoietic stem cell expansion: opposing roles of thrombopoietin and LNK. Genes Dev. 2006;20:2018–2023.
21. Okabe M, Ikawa M, Kominami K, Nakanishi T, Nishimune Y. 'Green mice' as a source of ubiquitous green cells. FEBS Lett. 1997;407:313–319.
22. Seita J, Ema H, Ooehara J, et al. Lnk negatively regulates self-renewal of hematopoietic stem cells by modifying thrombopoietin-mediated signal transduction. Proc Natl Acad Sci U S A. 2007;104:2349–2354.
23. Imai K, Kobayashi M, Wang J, et al. Selective transendothelial migration of hematopoietic progenitor cells: a role in homing of progenitor cells. Blood. 1999;93:149–156.
24. Osborn L, Hession C, Tizard R, et al. Direct expression cloning of vascular cell adhesion molecule 1, a cytokine-induced endothelial protein that binds to lymphocytes. Cell. 1989;59:1203–1211.
25. Avraham H, Cowley S, Chi SY, Jiang S, Groopman JE. Characterization of adhesive interactions between human endothelial cells and megakaryocytes. J Clin Invest. 1993;91:2378–2384.
26. Clarke MC, Savill J, Jones DB, Noble BS, Brown SB. Compartmentalized megakaryocyte death generates functional platelets committed to caspase-independent death. J Cell Biol. 2003;160:577–587.
27. Paulus JM, Debili N, Larbret F, Levin J, Vainchenker W. Thrombopoietin responsiveness reflects the number of doublings undergone by megakaryocyte progenitors. Blood. 2004;104:2291–2298.
28. Morino N, Mimura T, Hamasaki K, et al. Matrix/integrin interaction activates the mitogen-activated protein kinase, p44erk-1 and p42erk-2. J Biol Chem. 1995;270:269–273.
29. Chen Q, Lin TH, Der CJ, Juliano RL. Integrin-mediated activation of MEK and mitogen-activated protein kinase is independent of Ras. J Biol Chem. 1996;271:18122–18127.
30. Schulze H, Korpal M, Hurov J, et al. Characterization of the megakaryocyte demarcation membrane system and its role in thrombopoiesis. Blood. 2006;107:3868–3875.
31. Mattia G, Vulcano F, Milazzo L, et al. Different ploidy levels of megakaryocytes generated from peripheral or cord blood CD34+ cells are correlated with different levels of platelet release. Blood. 2002;99:888–897.

RhoH Plays Critical Roles in FcεRI-Dependent Signal Transduction in Mast Cells[1]

Hiroyo Oda,* Manabu Fujimoto,† Michael S. Patrick,*‡ Dai Chida,* Yoshinori Sato,* Yoshinao Azuma,‡ Hiroki Aoki,§ Takaya Abe,¶ Harumi Suzuki,[2]* and Mutsunori Shirai‡

RhoH is an atypical small G protein with defective GTPase activity that is specifically expressed in hematopoietic lineage cells. RhoH has been implicated in regulation of several physiological processes including hematopoiesis, integrin activation, and T cell differentiation and activation. In the present study, we investigated the role of RhoH in mast cells by generating RhoH knockout mice. Despite observing normal development of mast cells in vivo, passive systemic anaphylaxis and histamine release were impaired in these mice. We also observed defective degranulation and cytokine production upon FcεRI ligation in RhoH-deficient bone marrow-derived mast cells. Furthermore, FcεRI-dependent activation of Syk and phosphorylation of its downstream targets, including LAT, SLP76, PLCγ1, and PLCγ2 were impaired, however phosphorylation of the γ-subunit of FcεRI remained intact. We also found RhoH-Syk association that was greatly enhanced by active Fyn. Our results indicate that RhoH regulates FcεRI signaling in mast cells by facilitating Syk activation, possibly as an adaptor molecule for Syk. ***The Journal of Immunology*****, 2009, 182: 957–962.**

RhoH is a newly identified hematopoietic small G protein, originally cloned as one of the genes frequently disrupted in diffuse large B cell lymphoma (1, 2). Because RhoH is defective in GTPase activity and thus constitutively active, the function of this protein was thought to be regulated by its expression level. Overexpression of RhoH inhibited RhoA/Rac/cdc42-dependent NF-κB activation in HEK293 cells (3), and it also inhibited SCF-mediated Rac1 activation in bone marrow progenitor cells (4). Knockdown of RhoH increased spontaneous LFA-1-mediated adhesion in Jurkat cells (5), and in vitro colony formation in bone marrow progenitor cells (4). Recent studies, however, have demonstrated that RhoH plays critical roles in T cell development (6, 7) by functioning as an adaptor for ZAP-70 in TCR signaling (7) via its tyrosine-phosphorylated ITAM-like motif (8). In the absence of RhoH, development of T cells in the thymus is impaired in both β-selection and positive selection, resulting in a severe reduction of mature peripheral T cells (6, 7). RhoH-deficient T cells showed defective phosphorylation of LAT and ERK upon TCR stimulation, indicating that RhoH is critical in TCR-dependent proximal signal transduction events. The precise function of RhoH in TCR signaling, however, remains controversial because there is a discrepancy in the phosphorylation status of ZAP-70 between two reports (6, 7). Furthermore, the physiological function of RhoH in other hematopoietic lineage cells is largely unknown.

Mast cells are widely distributed in the body and function as the primary effectors in immediate-type hypersensitivity reactions (9, 10). Mast cells recognize Ags via IgE and specific, high-affinity Fc receptors, termed FcεRI (11–13). FcεRI cross-linking triggers activation of Src family kinases Lyn and Fyn, and phosphorylation of ITAM motifs on the γ subunit of FcεRI complexes (14, 15). Subsequently, ZAP-70-related Syk kinase binds to phosphorylated ITAM motifs of the γ subunit and is thus activated by Src kinases (16–18). Activated Syk, in turn, phosphorylates LAT, LAT-2, and SLP-76 to form the signalosome, which transduces signals downstream, initiating Ca^{2+} mobilization, degranulation, and the expression of specific genes (19–21). The FcεRI-initiated signal cascade in mast cells is analogous to the TCR-initiated signal cascade in T cells, sharing many common molecules and features (14, 15, 22). This prompted us to investigate the function of RhoH in FcεRI signaling in mast cells.

In this study, we report the critical role of RhoH in mast cell activation. We established RhoH-deficient mice to unveil the physiological roles of RhoH in mast cells. RhoH-deficient mice showed impaired passive systemic anaphylaxis (PSA)[3] and histamine release upon challenge with the specific Ag. Our in vitro data showing impaired Syk activation with defective degranulation and cytokine production in $RhoH^{-/-}$ mast cells supports the observed in vivo phenotypes. Furthermore, we demonstrated that RhoH associates with Syk, and this interaction was greatly enhanced in the presence of constitutively active Fyn. These results suggest that RhoH acts as a positive regulator for FcεRI-mediated signal transduction by facilitating Syk activation.

*Department of Pathology, Research Institute, International Medical Center of Japan, Tokyo, Japan; †Department of Dermatology, Kanazawa University Graduate School of Medical Science, Kanazawa, Japan; ‡Department of Microbiology, Yamaguchi University School of Medicine, Ube, Japan; §Cardiovascular Research Institute Kurume University School of Medicine, Kurume, Japan; and ¶Laboratory for Animal Resources and Genetic Engineering, Center for Developmental Biology, RIKEN Kobe, Japan

Received for publication January 16, 2008. Accepted for publication November 6, 2008.

The costs of publication of this article were defrayed in part by the payment of page charges. This article must therefore be hereby marked *advertisement* in accordance with 18 U.S.C. Section 1734 solely to indicate this fact.

[1] This work was supported by grants from the Ministry of Education, Culture, Sports, Science and Technology.

[2] Address correspondence and reprint requests to Dr. Harumi Suzuki, Department of Pathology, Research Institute, International Medical Center of Japan, 1-21-1 Toyama, Shinjuku, Tokyo, Japan. E-mail address: hsuzuki@ri.imcj.go.jp

[3] Abbreviations used in this paper: PSA, passive systemic anaphylaxis; BMMC, bone marrow-derived mast cell; HSA, human serum albumin; HA, hemagglutinin.

Materials and Methods

Mice

RhoH knockout mice (Acc.No.CDB0483K) were generated using the previously described methods (23, 24). In brief, the entire ORF of the *RhoH* gene located in the third exon was replaced with a cassette consisting of a *lacZ* and *neomycin* resistance gene (*LacZ/neo*) by homologous recombination. The lengths of the homologous regions in the targeting vector were 8.2 kb and 4.8 kb at the 5′ and 3′ sides of the DT-A/LacZ/neo cassette (http://www.cdb.riken.jp/arg/cassette.html), respectively. Two mutant mouse lines were established from two independent homologous recombinant ES cell lines; no difference was found in their phenotype. All mice were maintained after five generations of backcrossing to C57BL/6J (B6) and housed under specific pathogen-free conditions in accordance with institutional guidelines.

Mast cell culture

Bone marrow-derived mast cells (BMMCs) were prepared as described (25). In brief, femurs were isolated from 8- to 20-wk-old $RhoH^{+/+}$ and $RhoH^{-/-}$ mice, and BM cells were cultured in 2% conditioned RPMI 1640 medium from X63-IL-3 cells (gift from Dr. H. Karasuyama, Tokyo Medical and Dental University, Tokyo, Japan), containing 10% heat-inactivated FBS. After at least 4 wk of culture, cells were stained with PE-conjugated anti-FcεRI Ab and allophycocyanin-conjugated anti-c-*kit* Ab (BD Biosciences) and their expression was confirmed before use in all experiments.

Plasmids

Hemagglutinin (HA)-tagged RhoH cDNA was cloned into pcDNA3 vector using a PCR-based strategy from a mouse thymus cDNA library made in our laboratory. Myc-tagged Syk and active type Fyn cloned in pcDNA3 vector were kind from Dr. T. Kurosaki (RIKEN Research Center for Allergy and Immunology, Yokohama, Japan) and Dr. T. Yamamoto (Institute of Medical Science, University of Tokyo, Tokyo, Japan).

Passive systemic anaphylaxis

Mouse IgE anti-DNP (100 μg, clone SPE-7, Sigma-Aldrich) was administered i.v. through the tail vein in volumes of 300 μl/mouse. After 24 h, 100 μg of DNP-human serum albumin (HSA) in 300 μl of PBS was injected i.v. Immediately after Ag challenge, body temperature was measured every 5 min by rectal thermometer. At 30 min following Ag challenge, mice were sacrificed and peripheral blood was taken by cardiac puncture and plasma was used for histamine enzyme immunoassay (SPI-BIO).

Degranulation assay

BMMCs (5×10^4 per well) on 96-well plates were sensitized with 1 μg/ml IgE anti-DNP for 4 h at 37°C. Next, cells were washed three times with Tyrode's Buffer (130 mM NaCl, 5 mM KCl, 1.4 mM $CaCl_2$, 1 mM $MgCl_2$, 5.6 mM glucose, 0.1% BSA, 10 mM HEPES (pH 7.4)) and stimulated for 30 min with the indicated concentration of DNP-HSA or A23187 (200 ng/ml, Sigma-Aldrich) in 100 μl of Tyrode's buffer. Samples were centrifuged and supernatant was collected to measure the released β-hexosaminidase. To determine the total cell content of this enzyme, the cell pellet was lysed with 0.5% Triton X-100 in Tyrode's buffer and the lysate was collected. For each sample, 50 μl of substrate solution (1.3 mg/ml 4-nitrophenyl N-acetyl-β-D-glucosaminide in 0.1 M sodium citrate (pH 4.5); Sigma-Aldrich) was added and incubated for 1 h at 37°C. The reaction was stopped by the addition of 150 μl of 0.2 M glycine solution (pH 10.7). The absorbance at 405 nm was measured in a microplate reader (Bio-Rad).

Calcium flux assay

BMMCs were sensitized with 1 μg/ml IgE anti-DNP at 10^6/ml without IL-3 and labeled with 3 μM of Fura2-AM (Invitrogen) for 30 min at 37°C. Then, cells were washed three times and resuspended in Tyrode's buffer at 5×10^5/ml. Fluorescence intensities were measured at an excitation wavelength of 340 or 380 nm and an emission wavelength of 510 nm, with a fluorescence spectrometer (Hitachi F-2500) during stimulation as indicated in Fig. 5.

Real-time RT-PCR analysis

Total RNA was isolated from 10^6 stimulated or nonstimulated BMMCs (as described above) using RNeasy kit (Qiagen), and cDNA was generated using the SuperScript III kit (Invitrogen) according to the manufacturer's instructions. Real-time PCR was conducted using the Platinum SYBR Green qPCR Supermix (Invitrogen) with specific primers for RhoH (5′gatcaggagcaacctacc ct3′/5′atgcaggaagccctgtga3′), IL-6 (5′gctaccaaactggatataatcagga 3′/5′ccaggtag ctatggtactccagaa3′), TNF-α (5′tctctcattcctgcttgtgg3′/5′ggtctgggccatagaactga 3′), and β-actin (5′aaggccaaccgtgaaaagat3′/5′gtggtacgaccagaggcatac3′).

Immunoblotting and immunoprecipitation

For immunoblotting, BMMCs were sensitized with 1 μg/ml anti-DNP IgE at 10^6 cells/ml for 4 h without IL-3, washed three times, and then stimulated with DNP-HSA for the indicated periods. Stimulated BMMCs were lysed in lysis/wash buffer (1% Nonidet P-40, 150 mM NaCl, 50 mM Tris-Cl (pH 8.0), 1 mM sodium orthovanadate, 1 mM DTT, proteinase inhibitors), subjected to 7.5–12.5% SDS-PAGE and Western blotting (10^5 cells per lane). For FcRγ and Lyn, 10^6 BMMCs were lysed with lysis/wash buffer and immunoprecipitated with 1 μg of the indicated Abs, then subjected to 12.5% SDS-PAGE in tricine-SDS running buffer (0.1 M Tris, 0.1 M Tricine, 0.1% SDS for the upper chamber, 0.2 M Tris-Cl (pH 8.9) for the lower chamber), and Western blotting. For RhoH and Syk, 4.5×10^5 293T cells were transiently transfected with HA-tagged RhoH, myc-tagged Syk with or without constitutively active Fyn using FuGENE 6 (Roche). After 24 h, transfected cells were incubated with or without 30 μM PP2 (src kinase inhibitor) for 2 h before lysis. After 2 h, cells were lysed with magnesium containing lysis/wash buffer (1% NP40, 10 mM $MgCl_2$, 25 mM HEPES (pH 7.3), 150 mM NaCl, 8% glycerol, 1 mM EDTA, 1 mM sodium orthovanadate, and protease inhibitors), immunoprecipitated with 1 μg of the indicated Abs and then subjected to 12.5% SDS-PAGE in tricine-SDS running buffer. We confirmed that 30 μM of PP2 did not affect the overall tyrosine phosphorylation status of the cells, indicating that this concentration of PP2 specifically inhibits src kinases. Abs used for Western blotting and immunoprecipitation were anti-phospho Syk, -phospho PLCγ1, -phospho PLCγ2, -ERK, -phospho p38, -p38, -Lyn (Cell Signaling Technology), anti-phospho SLP76 and -phospho LAT (BD Biosciences), anti-phospho tyrosine (clone pY20, Neomarkers), anti-phospho tyrosine (clone 4G10), -myc and -HA (Roche) and -FcRγ (Millipore). We could not detect endogenous RhoH using commercially available or in-house generated RhoH Abs from rabbit or rat.

Histochemistry

To observe tissue mast cells, 6-μm paraffin sections of fixed tissues were stained with toluidine blue (Sigma-Aldrich) and the total number of mast cells in each tissue unit was counted. A skin unit was defined as the entire area of an ear section along the cartilage, and a stomach unit was defined as the entire area of a sagittal section.

Results

Generation of $RhoH^{-/-}$ mice

Mice carrying a mutant *RhoH* allele were generated from TT2 embryonic stem cells in which homologous recombination was used to replace the entire coding region located in exon 3 of the *RhoH* gene. As a result, there is no possibility of expression of any truncated forms of the protein in the mice (Fig. 1*A*). Offspring carrying the mutant allele were identified by Southern blotting (Fig. 1*B*). Homozygous *RhoH*-null mice were born at the expected Mendelian ratio.

Impaired FcεRI-mediated anaphylaxis in $RhoH^{-/-}$ mice

We found that RhoH is expressed in mast cells as well as T and B cells (Fig. 1*C*), as previously reported (4). Because the role of RhoH in immune cells other than T cells has not been characterized, we focused on mast cells in the present study. One of the major functions of mast cells is inducing allergy and anaphylaxis, therefore, we examined PSA, in which exogenously administered IgE is passively taken up by mast cells and degranulation is evoked by subsequent administration of Ag. As shown in Fig. 2*A*, the IgE-dependent PSA response in $RhoH^{-/-}$ mice, evaluated by the reduction of core body temperature after DNP-HSA injection, was smaller compared with those in $RhoH^{+/+}$ mice. As shown in Fig. 2*B*, measurement of plasma histamine concentration 30 min after DNP-HSA challenge revealed reduced secretion of histamine in $RhoH^{-/-}$ mice compared with $RhoH^{+/+}$ mice. Collectively, we demonstrated that RhoH is important in the systemic anaphylaxis reaction in vivo.

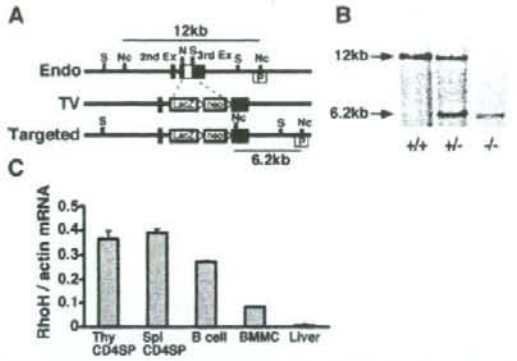

FIGURE 1. Generation of RhoH$^{-/-}$ mice. *A*, Targeting vector was designed to disrupt the *RhoH* gene by homologous recombination. The endogenous locus of *RhoH* (Endo), targeting vector (TV), and targeted locus (Targeted) are shown. The open box in the third exon represents the entire ORF of *RhoH* that was replaced by a *LacZ/neomycin* resistance gene. Restriction sites are abbreviated as follows: S, *Sal*I; Nc, *Nco*I; N, *Not*I. P in the open box indicates the location of probe for Southern blotting. *B*, Southern blot analysis of *Nco*I digested mouse genomic DNA. A 12- and 6.2-kb band represent the wild-type and targeted alleles, respectively. *C*, Expression of RhoH mRNA was detected by real time RT-PCR in the indicated cells and tissues. Results are the mean and SE from three independent experiments, $n = 9$ for each group.

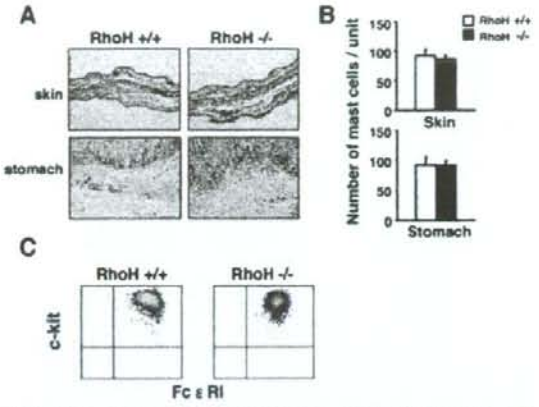

FIGURE 3. Normal development of mast cells in RhoH$^{-/-}$ mice. *A*, Mast cells in the ear skin (*upper*) and stomach (*lower*) in RhoH$^{+/+}$ and RhoH$^{-/-}$ mice were detected with toluidine blue staining. The highly metachromatic cells are mast cells. *B*, Number of mast cells in indicated tissues. Results are the mean and SE of mast cells per unit from indicated number of mice. For ear skin, $n = 4$ mice per group; for stomach, $n = 3$ per group. *C*, Expression of FcεRI and c-*kit* on the surface of BMMCs induced from RhoH$^{+/+}$ and RhoH$^{-/-}$ mice was analyzed by flow cytometry. Shown are representative data from more than five independent experiments.

Normal development of mast cells in RhoH$^{-/-}$ mice

Because we found impaired anaphylaxis in RhoH-deficient mice, we assessed the effect of RhoH disruption on mast cell development in vivo. Histological analysis by toluidine blue staining demonstrated that the anatomical distribution and morphology of connective tissue mast cells in the skin and mucosal mast cells in the stomach of RhoH$^{-/-}$ mice were comparable to those of RhoH$^{+/+}$ mice (Fig. 3*A*). The number of mast cells detected per area in these tissues was not changed in these mice (Fig. 3*B*). Growth rate and total number of in vitro induced BMMCs from RhoH-deficient mice were comparable to those from RhoH$^{+/+}$ mice (data not shown). After 4 wk culture, the proportion of FcεRI and c-*kit* double positive cells was >95% in both RhoH$^{-/-}$ and RhoH$^{+/+}$ BMMCs (Fig. 3*C*). From these results, we conclude that RhoH is dispensable for mast cell development both in vivo and in vitro.

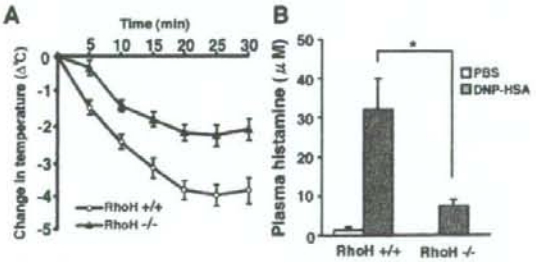

FIGURE 2. Impaired systemic anaphylaxis in RhoH$^{-/-}$ mice. *A*, RhoH$^{+/+}$ (○) and RhoH$^{-/-}$ (▲) mice were sensitized with anti-DNP IgE overnight, then challenged with DNP-HSA (100 μg), and the core body temperature was measured up to 30 min. Representative data of three independent experiments is shown. *B*, At 30 min after induction of PSA, peripheral blood was taken from RhoH$^{+/+}$ and RhoH$^{-/-}$ mice by cardiac puncture and the plasma histamine concentration was measured by EIA. Results are the mean and SE from three independent experiments. Statistical significance was determined by Welch's *t* test; *, $p < 0.05$. $n = 5$ control mice, $n = 6$ knockout mice.

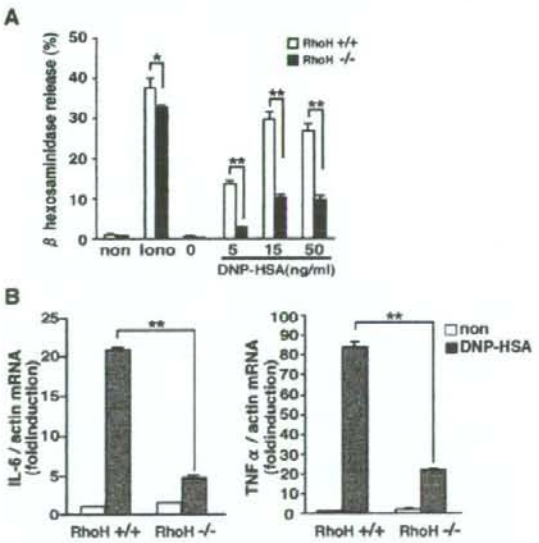

FIGURE 4. FcεRI-stimulated degranulation and cytokine production were impaired in RhoH$^{-/-}$ mast cells. *A*, BMMCs from RhoH$^{+/+}$ (□) and RhoH$^{-/-}$ (■) were sensitized with anti-DNP IgE, then 30 min after DNP-HSA (at the indicated concentrations) or A23187 (Iono, 200 ng/ml) stimulation, degranulation was assayed by β-hexosaminidase release. *B*, Anti-DNP IgE-sensitized BMMCs were stimulated with DNP-HSA (10 ng/ml) for 1 h or unstimulated. Then, IL-6 (*left*) and TNF-α (*right*) mRNA were quantified by real time RT-PCR. Results are the mean and SE from three independent experiments; $n = 9$ for each group. Statistical significance was determined by Student's *t* test; *, $p < 0.05$; **, $p < 0.01$.